Detecting rate changes in spike trains

Diplomarbeit
Eingereicht am Institut für Mathematik, Schwerpunkt Stochastik
Fachbereich Informatik und Mathematik
der J.W. Goethe-Universität Frankfurt am Main

von
Marietta Tillmann

Betreuerin:
JProf. Dr. Gaby Schneider

04.02.2010

Zusammenfassung

Neurone sind elementare Bausteine des Gehirns, welche über Synapsen kommunizieren und auf diese Weise ein kompliziertes Netzwerk bilden. Informationen werden über Aktionspotentiale (Spikes) ausgetauscht, welches Alles-Oder-Nichts-Reaktionen sind und somit ununterscheidbar abgesehen von dem Zeitpunkt ihres Auftretens. Hat man eine Sequenz von Aktionspotentialen, Spike train genannt, so kann man jeden Spike als Punkt auf der Zeitachse betrachten und somit den Spike train als Realisierung eines Punkt Prozesses.
Der Analyse von Spike trains liegen oft Stationaritätsannahmen zugrunde, was bedeutet, dass die Parameter des Punkt Prozesses als konstant über die Zeit angenommen werden. Dabei bezieht sich diese Annahme meistens auf die Feuerrate, also auf die Frequenz mit der die Spikes auftreten. Die Analysen werden dadurch vereinfacht, was allerdings zu falschen Ergebnissen bzw. Interpretationen führen kann. Zum Beispiel kann Nichtstationarität manchmal der einzige Grund für Korrelationen zwischen Spike trains sein (Brody, 1999).
Für die Prüfung der Stationaritätsannahme existieren heute zwar verschiedene Techniken, jedoch finden diese Tests noch wenig Anwendung in der Praxis, was zum Teil auf ihre praxisuntauglichkeit und geringe Testmacht zurück zu führen ist (Gourevitch and Eggermont, 2007). Das Ziel dieser Arbeit ist es, konkrete Zeitpunkte der Ratenwechsel zu identifizieren. Dies würde es ermöglichen, den Spike train in Teile zu separieren, wo Stationarität der Feuerrate angenommen werden kann. Für die Analyse werden folgende Annahmen getroffen:

1. ein Spike train kann als Poisson Prozess mit Parameter $\lambda(t)$ beschrieben werden

2. die Intensität $\lambda(t)$ (Feuerrate) kann durch eine Treppenfunktion approximiert werden

Im Rahmen dieser Arbeit konnte eine Methode entwickelt werden, welche es ermöglicht, unter den oben getroffenen Annahmen Ratenveränderungen zu lokalisieren. Diese Methode, Stufen-Filter-Test (SF-Test) genannt, wird im ersten Teil der Arbeit vorgestellt und soll hier nachfolgend zusammen gefasst werden. Um ein vollständiges Bild der Forschungsarbeit zu geben, werden im zweiten Teil der Arbeit die Ansätze präsentiert, die dem SF-Test vorangegangen sind, allerdings das Ziel der Detektierung konkreter Ratenwechsel verfehlt haben. Diese Verfahren liefern interessante Illustrationen des Verlaufs der Intensität und ermöglichen subjektive Aussagen im Bezug auf die Zeitpunkte der Intensitätsänderungen. Jedoch ist eine fundierte statistische Analyse erst durch den SF-Test gegeben.

Lokalisation von Intensitätsänderungen – Der Stufen-Filter-Test

Betrachtet man einen Spike train der Länge $T[s]$ unter der Annahme, dass die Wartezeiten (Interspike-Interval = ISI) exponentialverteilt sind, so ist die erwartete Anzahl N der Spikes in einem Intervall der Länge h gegeben durch $E[N] = \lambda(t)h$. Ist nun die Feuerrate konstant über die Zeit, $\lambda(t) \equiv \lambda$, so gilt für die Differenz von Spike-Anzahlen in benachbarten Intervallen der Länge h, $[t-h, t)$ und $[t, t+h]$ mit $t \in [h, T-h]$, $E[N_1 - N_2] = 0$ mit Standardabweichung $\sqrt{2h\lambda}$. Ändert sich die Rate zum Zeitpunkt $\frac{T}{2}$ so verhält sich die Differenz der Spike-Anzahlen wie im konstanten Fall, falls beide Intervalle in dem ersten oder in dem zweiten Teil des Spike trains liegen. Ansonsten, für $t \in [\frac{T}{2} - h, \frac{T}{2} + h]$, findet man $E[N_1 - N_2] = (E[N_1] - E[N_2]) \neq 0$.
Führt man dies für ein festes h systematisch durch, so kann man jedem Zeitpunkt $t \in [h, t-h]$ einen Wert für die Differenz, normiert durch die Standardabweichung der Differenz $\sqrt{2h\hat{\lambda}}$ mit $\hat{\lambda} = \dfrac{N(t-h, t+h)}{2h}$, zuordnen. Die Test-Statistik ist somit definiert durch:

$$D_{h,t} = \frac{(N_1 - N_2)}{\sqrt{2h \cdot \frac{(N_1+N_2)}{2h}}} = \frac{(N_1 - N_2)}{\sqrt{(N_1 + N_2)}}$$

mit N_1, N_2 unabhängig und poissonverteilt. Um Aussagen über die beobachtete Dif-

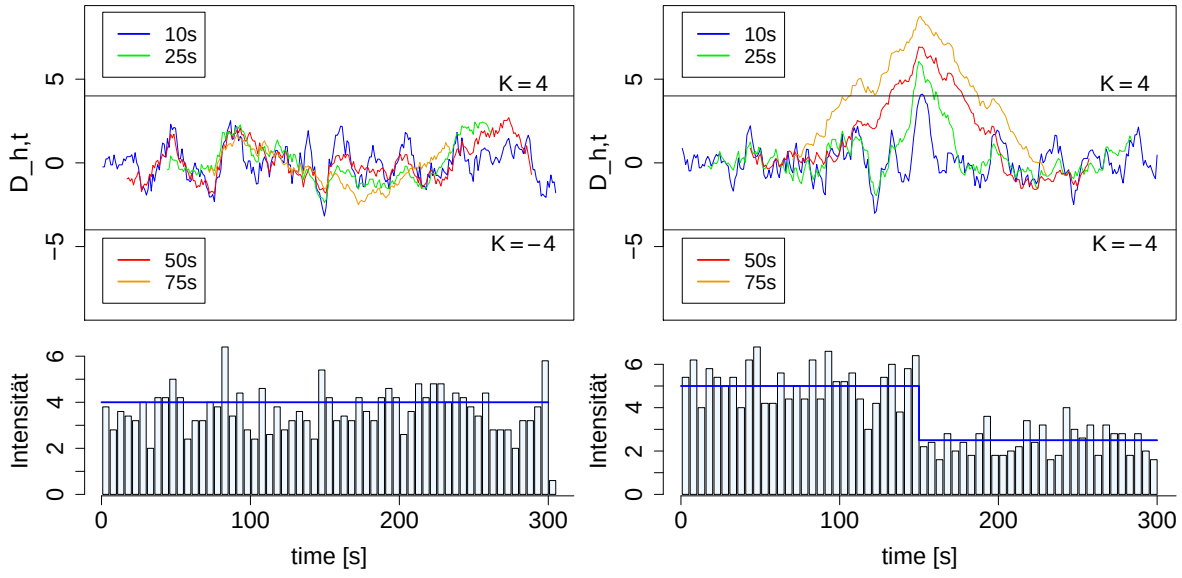

ferenz zwischen N_1 and N_2 im Bezug auf das Vorliegen eines Ratenwechsels treffen zu können, braucht es eine Entscheidungsregel. Seien $N_1 \sim \text{Pois}(\lambda_1 \text{h})$ und $N_2 \sim \text{Pois}(\lambda_2 h)$. Die Null-Hypothese H_0, $\lambda_1 = \lambda_2$, wird abgelehnt zugunsten der Alternativhypothese H_1, $\lambda_1 \neq \lambda_2$, wenn $D_{h,t}$ außerhalb eines kritischen Bereichs fällt, sprich $|D_{h,t}| > K$. Für den kritischen Wert K erhält man unter der Bedingung, dass in 1000 simulierten

Poisson Prozessen der Länge $T = 700s$ mit Parameter λ nur in 10 Fällen $|D_{h,t}| > K$ beobachtet wird, approximativ $K = 4$. Dabei ist K nicht nur abhängig von T sondern auch von h, denn diese beiden Größen legen die Anzahl der Zeitpunkte t fest, für die $D_{h,t}$ ausgewertet werden kann. So ist diese Anzahl zum Beispiel für kleine Fenstergrößen höher und somit die Wahrscheinlichkeit größer, dass $|D_{h,t}| > K$ eintritt. Hier wurde $K = 4$ mittels der Fensterbreiten bestimmt, welche auch später in der Anwendung der Methode genutzt werden (s. Abb. oben).

Für die Evaluation der Testmacht zeigt man zunächst mittels δ-Methode, dass $D_{h,t}$ asymptotisch normalverteilt ist mit asymptotischen Erwartungswert μ und asymptotischer Varianz σ^2

$$\mu = \frac{(\lambda_1 - \lambda_2)}{\sqrt{\lambda_1 + \lambda_2}} \cdot \sqrt{h} \quad \text{und} \quad \sigma^2 = 1 - \frac{3}{4}\frac{(\lambda_1 - \lambda_2)^2}{(\lambda_1 + \lambda_2)^2}.$$

Geht man von einem Ratenwechsel zum Zeitpunkt h aus, so dass $[0, h]$ und $[h, 2h]$ jeweils einen Abschnitt mit konstanter Rate umfassen mit $\lambda_1 > \lambda_2$, so gilt für die Wahrscheinlichkeit, dass $D_{h,t}$ unter H_1 außerhalb des Bereichs $[-4, 4]$ fällt, asymptotisch

$$P(D_{h,h} > 4) \approx 1 - \Phi\left(\frac{4 - \mu}{\sqrt{\sigma^2}}\right).$$

Die Testmacht ist somit abhängig von den drei Größen h, λ_1, λ_2 mit den folgenden Beziehungen:

1. Für festes λ_1 und λ_2: je größer h desto größer die Testmacht
2. Für festes λ_1 und h: je größer $|\lambda_1 - \lambda_2|$ desto größer die Testmacht
3. Für festes $|\lambda_1 - \lambda_2|$ und h: je kleiner λ_i desto größer die Testmacht

Vor der Anwendung der Methode wurden noch drei Größen festgelegt:

1. Die Wahl der Fensterbreite h

Dabei muss man abwägen zwischen kleinen Fensterbreiten, welche es ermöglichen kurze Zeitabschnitte mit konstanter Rate zu identifizieren und großen Fensterbreiten, welche bei genügend langer Dauer von Abschnitten mit konstanter Rate die Testmacht erhöhen. In der vorliegenden Arbeit wurde für die Durchführung der Methode $h = 10s, 25s, 50s, 75s, 100s, 125s, 150s$ gewählt. Diese Wahl beruht zum einen darauf, dass in den Daten Raten mit $0.8 < \lambda_i < 8$ beobachtet wurden und somit die Testmacht für die meisten Ratenkominationen von λ_1 und λ_2 mit $h \leq 150s$ mindestens 80% beträgt. Zum anderen müssten, damit man mit $h > 150s$ Ratenwechsel identifizieren kann, die entsprechenden Abschnitte im Spike train länger als $150s$ sein, was in den Daten selten beobachtet werden konnte. Als kleinste Fensterbreite wurde $h = 10s$ gewählt, da für kleinere Fensterbreiten wie $h = 5s$ kaum

ein Ratenunterschied eine hohe Wahrscheinlichkeit hat entdeckt zu werden.

2. Identifikation des Schätzers für den Zeitpunkt des Ratenwechsels
Liegt ein Ratenwechsel zum Zeitpunkt t_c[1] vor, so erreicht $E[D_{h,t}]$ für ein festes h sein Maximum am Zeitpunkt des Ratenwechsels d.h. $\max_t(E[D_{h,t}]) = E[D_{h,t_c}]$. Der Schätzer $\hat{t}_c$ wurde definiert als der Zeitpunkt t mit $\max_t(E[D_{h_{min},t}])$, wobei h_{min} die kleinste Fenstergröße ist, die $|D_{h,t}| > 4$ beobachtet hat. Nach der Identifikation der t_{c_i}, kann die Intensität durch eine Treppenfunktion approximiert werden, indem in jedem Ratenabschnitt die Intensität durch die mittlere Spike-Anzahl geschätzt wird.

3. Evaluation der Qualität des Schätzers
Die Genauigkeit des Schätzers wurde in Simulationen bestimmt. Es konnte beobachtet werden, dass der Schätzer für festes λ_1 umso genauer ist, je größer $|\lambda_1 - \lambda_2|$. Andererseits ist für festes $|\lambda_1 - \lambda_2|$ der Schätzer genauer für niedrige Raten, also für größere relative Differenzen zwischen λ_1 und λ_2.

Anwendung des SF-Tests

Die Methode wurde zunächst auf simulierte Spike trains mit exponentialverteilten ISIs angewandt, wobei die Intensität als Treppenfunktion modelliert wurde. Die simulierten Ratenwechsel konnten in vielen Fällen zuverlässig gefunden werden. Die Voraussetzung für die Detektion war eine genügend große Testmacht, wobei hier das gegenseitige Bedingen der drei Einflussgrößen der Testmacht eine Rolle spielt. So ist zum Beispiel für $|\lambda_1 - \lambda_2| < 1$ bei gleichzeitigem Vorliegen von kurzen Zeitabschnitten mit konstanter Rate die Wahrscheinlichkeit gering, dass der Test anschlägt. Dies kann darauf zurück geführt werden, dass solche Unterschiede in der "intrinsischen" Variabilität des Poisson Prozesses untergehen, wobei die Variabilität bei größeren Raten λ_i höher ist.
Die Anwendung auf die realen Daten ergab, dass die Methode plausible Ratenwechsel findet und somit das Schätzen der Ratenfunktion gemäß einer Stufenfunktion ermöglicht. Schwierigkeiten bereiten abfallende bzw. ansteigende Intensitäten, da die Testmacht für geringe Unterschiede zwischen den Raten und kleinen h sehr gering ist. Hier ist allenfalls eine grobe Approximation der Intensität durch wenig Stufen möglich, falls die Dauer, in der die Rate kontinuierlich abfällt (ansteigt), nicht zu kurz ist.

[1] Der Index c steht hier für "change"

Ausblick

Der Stufen-Filter-Test stellt eine Möglichkeit dar, konkrete Zeitpunkte von Ratenveränderungen zu detektieren und somit den Spike train in Bereiche einzuteilen, in denen eine konstante Rate angenommen werden kann unter der Annahme, dass die ISIs exponentialverteilt sind. Auf dieser Grundlage könnten nachfolgende Analysen des Spike trains durchgeführt werden.
Allerdings ist die Annahme von exponentialverteilten ISIs nicht für jeden Spike train geeignet. Allgemeiner kann man von gammaverteilten ISIs ausgehen, so dass durch den zusätzliche Parameter κ eine größere Breite von Spike trains angepasst werden kann, wobei $\kappa > 1$ ein regelmäßigeres Auftreten der Aktionspotentiale impliziert. Hier müsste man allerdings für jedes κ eine neue Schranke K definieren. Dabei kann für $\kappa > 1$ ein kleinerer Annahmebereich der Nullhypothese erwartet werden, da die Anzahl der Spikes weniger variabel ist. Somit dürften durch die angepassten Schranken mehr Ratenwechsel gefunden werden als unter der Poisson-Annahme. Ein Problem ist hierbei, dass K abhängig wäre von dem Parameter κ, welcher bei Nichtstationarität nicht zwangsläufig als konstant angenommen werden kann über die Zeit (Shimokawa et al., 2009).

Contents

List of Figures

List of Tables

1 Introduction

Neuronal activity in the brain is often investigated in the presence of stimuli, termed externally driven activity. This stimulus-response-perspective has long been focussed on in order to find out how the nervous system responds to different stimuli. The neuronal response consists of baseline activity, so called spontaneous activity[1], and activity which is caused by the stimulus. The baseline activity is often considered as constant over time which allows the identification of the stimulus-evoked part of the neuronal response by averaging over a set of trials.

However, during the last years it has been recognized that own dynamics of the nervous system plays an important role in information processing. As a consequence, spontaneous activity is no longer regarded only as background 'noise' and its role in cortical processing is reconsidered. Therefore, the study of spontaneous firing pattern gains more importance as these patterns may shape neuronal responses to a larger extent as previously thought. For example, recent findings suggest that prestimulus activity can predict a person's visual perception performance on a single trial basis (Hanslmayr et al., 2007). In this context, Ringach (2009) remarks that one can learn much about even the quiescent state of the brain which "underlies the importance of understanding cortical responses as the fusion of ongoing activity and sensory input".

Taking into account that spontaneous activity reflects anything else but noise, new challenges arise when analysing neuronal data. In this thesis one of these problems related to the analysis of neuronal activity will be adressed, namely the nonstationarity of firing rates.

The present work consists of four chapters. First of all the introduction gives neurophysiological background information to get an idea of neuronal information processing. Afterwords the theory of point processes is provided which forms the basis for modeling neuronal spiking data. In the last section of the introduction a statement of the problem is given. Chapter 2 proposes an easily applicable statistical method for the detection of nonstationarity. It is applied to simulations and to real data in order to show its capabilities. Thereafter, four other approaches are presented which provide

[1] Spontaneous activity is defined as the firing of neurons in the absence of sensory input (Ringach, 2009)

useful illustrations concerning the nonstationarity of the firing rate but share the problem that one cannot make objective statements on the basis of their results. They were developed in the course of establishing a suitable method. In chapter 4 the results are discussed and suggestions for further study are given.

1.1 Neurophysiological background

Neurons are nonlinear elements which generate electrical pulses, called spikes or action potentials. Neurons are connected to each other by synapses building a neuronal network. Spikes are used to signal over distances respectively to exchange information between the neurons. The signal output of a neuron is sent out along its axon to other neurons to which it is connected. If the postsynaptic potential – the sum of all excitatory and inhibitory input signals – exceeds a given threshold then the target neuron generates an action potential. But if the excitation is below the threshold the neuron will not fire. Therefore, an action potential is called an all or nothing event: "[...] this signal does not occur at a subthreshold electric excitation, but fully occurs at a superthreshold excitation" (Haken (2008), p. 11). As a consequence, the shape of the action potential, the intensity and duration of the spike, is the same regardless of the amount of excitation received from the inputs. Thus, spikes of a single neuron can be treated as unitary pulses which differ from each other only in respect of the timepoints at which they occur.

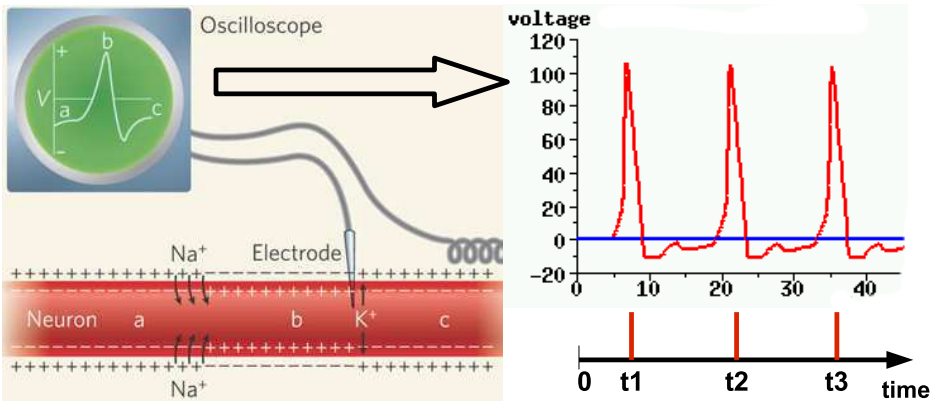

Figure 1.1: Recording of action potentials (AP) and the transformation of their detailed voltage waveform in a more simple representation so that the AP is reduced to its main information, speak its occurence on the time axis (modified according to Gutkin and Ermentrout (2006), p. 999).

A sequence of action potentials, recorded over a finite time period, forms a spike train. Given that the shape of action potentials does not differ their detailed voltage waveform can be neglected when depicting a spike train on the time axis (see figure 1.1). Only the time of arrival of an action potential, which distinguishes it from the others, is of interest and focussed on when spike trains are analysed. Thereby the timepoint can be associated with "the time of maximum excursion of electrical potential, which can be measured with a high degree of precision" (Perkel et al. (1967), p. 393). Technically the occurrence of a spike is an event. So a spike train can be considered as a sequence of finitely many events which occur at specific points in time. In the next paragraph the statistics of such events will be adressed for a better understanding of spike train analysis.

1.2 Mathematical background

Stochastic point processes are often applied as mathematical models for neuronal spiking. The events are identified as the occurrence times of the spikes (spike times) whose other characteristics, e.g. duration or amplitude, are ignored. The statistic of the intervals between successive events is important in characterizing the process: "In any point process, in which all 'events' (spikes, for example) are indistinguishable except for their times of occurrence, it is the elapsed times between events, e.g. the interspike intervals, that exhibit the properties of random variables. These intervals are regarded as being drawn [...] from an underlying probability distribution" (Perkel et al. (1967), p. 394). In this section the mathematical framework for the analysis of neuronal spiking data is provided. First, a definition of stochastic processes is given before the theory of point processes is addressed which forms the foundation for modeling spike train data.

Definition 1.2.1 (Stochastic process) *A stochastic process* $(\mathbf{X}_t)_{t\in\mathcal{T}}$ *with state space* S *is a family of* S*-valued random variables* $\mathbf{X}_t$ *indexed by a set* $\mathcal{T}$ *(*t *can be interpreted as time) with*
a) $\mathcal{T} = \{0, 1, 2, ...\} \Rightarrow$ *discrete time stochastic process*
b) $\mathcal{T} = [0, \infty) \Rightarrow$ *continuous time stochastic process*
Thereby $(\mathbf{X}_t)_{t\in\mathcal{T}}$ *is a discrete-state process if its values are countable, otherwise it is a continuous-state process.*

In the following $\mathcal{T}$ equals $[0, \infty)$ as continuous time is needed for the concept of point processes which provide useful conceps when analysing spike trains.

Definition 1.2.2 (Point process) *A point process is a continuous time stochastic process whose realizations consist of a series of point events occurring at well defined but random points in time.*

So a point process can be considered as a random collection of points t_i, where each point represents the time of an event on the time axis. Apart from their times, the points are thought to be indistinguishable. The theory of point processes is used to describe data, like neuronal signals, that are localized at a finite set of timepoints.
To every point process a discrete-state stochastic process $\mathbf{N}(t)$ in continuous time can be associated by counting the number of events as they come along. Thereby $\mathbf{N}(t)$ denotes the number of points in the time interval $[0, t]$.

Definition 1.2.3 (Counting Process) *A counting process* $\{\mathbf{N}(t), t \in \mathcal{T}\}$ *is a stochastic process in continuous time that counts the number of events* t_i *which occurred up to and including a specific moment of time:* $\mathbf{N}(t) = max\{i : t_i \leq t\}$.

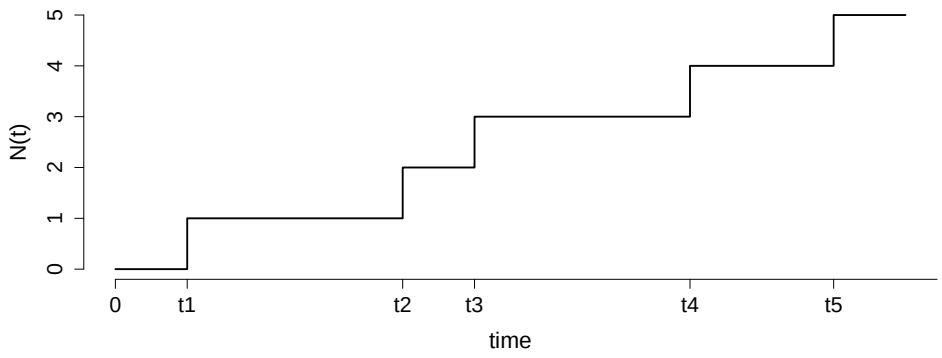

Figure 1.2: Illustration of a counting process: $\mathbf{N}(t)$ equals the number of points t_i up to time t.

$\mathbf{N}(t)$ is well defined at any time t. It is constant between the events and increases in unit steps at each time point t_i (see figure 1.2). So $\mathbf{N}(t)$ is non decreasing and piecewise constant. For $s < t$, $\mathbf{N}(s, t) = \mathbf{N}(t) - \mathbf{N}(s)$ denotes the number of events in the half-open interval $(s, t]$.
A simple example for a continuous-time counting process is the Poisson Process which often forms the basis for many more complex models.

Definition 1.2.4 (Poisson process) *A Poisson process is a continuous-time counting process* $\{\mathbf{N}(t), t \in \mathcal{T}\}$ *which possesses the following properties*

1. $\mathbf{N}(0) = 0$

2. *The probability distribution of* $\mathbf{N}(t)$ *events up to time* t *is poisson*
3. *The probability distribution of the waiting times* $\mathbf{Y}_i$ *is exponential*
4. $\mathbf{N}(t)$ *has independent increments*
5. *Multiple occurrences at the same* t *may not occur*

The intensity function $r(t)$ of a Poisson process can be interpreted as the rate at which points occur in a small interval at time t. So more points occur when $r(t)$ is relatively high. A stationary (homogeneous) Poisson process is characterized by a constant rate parameter $r(t) \equiv \lambda$ which indicates the expected number of events per time unit. This implies that $\mathbf{N}(t, t+\tau) = \mathbf{N}(t+\tau) - \mathbf{N}(t)$, the number of events in the time interval $(t, t+\tau]$, is Pois$(\lambda\tau)$-distributed. Thus, the probability of k events being in the interval $(t, t+\tau]$ is given by the equation

$$P(\mathbf{N}(t, t+\tau) = k) = \frac{1}{k!}(\lambda\tau)^k e^{\lambda\tau}.$$

Thus, the expected number of occurrences in that time interval is $E[\mathbf{N}(t, t+\tau)] = \lambda\tau$ with variance $\mathrm{Var}[\mathbf{N}(t, t+\tau)] = \lambda\tau$.
In a stationary Poisson process with parameter λ the interarrival times $\mathbf{Y}_i$ between successive events t_i and t_{i+1} are Exp(λ)-distributed. This means that $\mathbf{Y}_i$ has the probability density function

$$f(x) = \begin{cases} \lambda e^{-\lambda x} & \text{for} \quad x \geq 0 \\ 0 & \text{for} \quad x < 0. \end{cases}$$

So the expected waiting time and its variance are given by

$$E[\mathbf{Y}_i] = \frac{1}{\lambda}$$
$$\mathrm{Var}[\mathbf{Y}_i] = \frac{1}{\lambda^2}.$$

However, the rate may change over time. In this case the process, called nonstationary (inhomogeneous) Poisson process, is characterized by a generalized rate function $r(t)$ which is now a more complex function than a constant one. The expected number of events between time t and time s is then given by the integral $\lambda_{t,s} = \int_t^s r(t)\, dt$.

1.3 Statement of the problem

Spike trains are often considered to arise from stationary point processes which means that the parameters of the process are invariant under time shift. Note that the detection and measurement of stationarity is focussed almost exclusively upon one parameter,

namely the firing rate, so that the assumption of stationarity implies that the intensity of spiking is constant over time (Perkel et al., 1967). But the behaviour of a neuron can change during the course of observation. For example, accelerations (decelerations) or jumps in the intensity destroy the notion of an underlying stationary point process so that the average firing rate has to be interpreted with care as it does not represent every part of the record equally well.

However, most of the models and statistical measures carry the implicit assumption that the underlying point process is stationary and therefore oversimplify the statistics of the target spike train. As a consequence, interpretational ambiguity may arise which can lead to biased results in several signal analysis methods such as the peristimulus time histogramm (PSTH) which is the average response over a set of trials (repeatedly presented identical stimulus). Nonstationarity of the firing rate across trials causes that the PSTH is not representative of each individual trial and therefore leads to deceptive conclusions. Similarly, the cross-correlogram, which is used to detect interactions between spike trains, can provide misrepresentations of the results when the spike trains are composed of inhomogeneous point processes. Strictly speaking, nonstationarities can also cause correlations so that peaks in the correlogram are not always indicative of spike timing synchronization between neurons (Brody, 1999). Hence the need for preprocessing methods in order to check whether the assumption of stationarity is reasonable.

Note that the problem of nonstationarity has long been known. Already Perkel et al. (1967) drew attention to the importance of searching for conspicuous changes in the intensity of spiking. Indeed, the problem is still relevant today whereby scientists have made progress concerning the handling of rate variations. Gourevitch and Eggermont (2007) give an overview of the existing techniques from visual inspection of interspike intervals to different tests some of which they rated as not very powerful. However, most of the methods only allow to decide whether the assumption of an underlying stationary point process is reasonable for the data and not to locate the corresponding change points. If a method provides a change point analysis then it works under strict conditions like the assumption of only one rate change. Further need for research is given, so that simple and practical methods can be established which are able to locate changes in the intensity without making assumptions about the number of changes.

In this diploma thesis we pursue the goal of detecting change points in the firing rate in order to identify parts of the spike train where the assumption of stationarity is justified. Therefore, some theoretical approaches have been developed which are presented in two separated chapters. First, the main method is introduced which enables us to pinpoint rate changes under the assumption that the ISIs are exponential distributed. As a result, it provides an approximation of the intensity by a step rate function (SRF).

Second, a compilation of other techniques is given which were developed while working on a practical method. They are useful in order to depict the course of the intensity but lack a statistical foundation.

1.3.1 Simulation of spike trains on the basis of Poisson processes

In order to evaluate the theoretical results spike trains composed of Poisson processes are simulated. Therefore, the spike train is considered as a realization or sample function of a continuous time Poisson process which means that it is viewed as a point pattern on $[0, \infty)$ whereby the interarrival times are $\text{Exp}(\lambda)$-distributed and the points conveniently represent the spike times.
Note that it is not always possible to approximate a spike train by a Poisson process. More generally a gamma distribution, which shows a refractory period[2] and firing patterns of different regularity, was observed to be "a more realistic description of interval statistics than the more commonly used Poisson process [...]" (Baker (2000), p. 650). The shape parameter κ allows for the adjustment of regularity of the corresponding spike train in the following way (Nawrot et al. (2008), Baker (2000)):

1. For $\kappa = 1$ the ISIs are exponentially distributed $\Rightarrow$ Poisson process
2. For $\kappa > 1$ the process is more regular
3. For $0 < \kappa < 1$ the process is more irregular so that "events appear clustered in time" (Nawrot et al. (2008), p. 375)

In this diploma thesis we use the Poisson model as a first approximation, which enables us to develop an easily applicable method for the detection of rate changes as it is $\kappa \equiv 1$, so that only one time dependend parameter $\lambda(t)$ has to be taken into account. In the following the mathematical characterization of a spike train is given in order to introduce basic terminology which will be used in the next chapters.
Let t_i be the occurrence time of the ith spike in a spike train of M spikes recorded between 0, onset of the recording, and T seconds. So $N(T)$, the number of events until time T, is $N(T) = M$. Dividing the recording in n intervals of $h = \frac{T}{n}$ seconds, the number of spikes in a single time interval is given by $N_i = N(h_{i-1}, h_i) = N(h_i) - N(h_{i-1})$ with $h_i = i \cdot h$, $i = 1, \ldots, n$. This construction yields a discrete-time representation of a point process which is needed for the development of data analysis methods.

[2] After the initiation of an action potential, the refractory period is defined as the interval during which a second action potential cannot be initiated

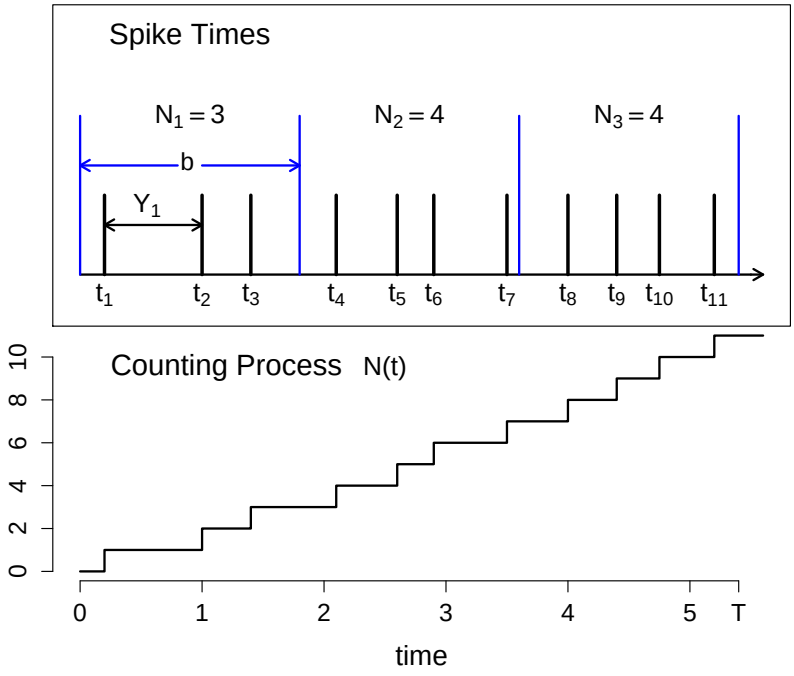

Figure 1.3: Discretization of neuronal data by dividing the spike train in intervals of h seconds (here: $M = 11$, $T = 5.4$, $n = 3$, $h = 1.8$).

Under the assumption that the spike train is a homogeneous Poisson process with rate parameter λ it is known that the number of spikes in an interval of h seconds is Pois(λh)-distributed. Therefore λh spikes are expected in every interval, whereby the number of observed occurrences in a single interval fluctuates with standard deviation $\sqrt{\lambda h}$. In addition the interspike intervals (ISIs) $\mathbf{Y}_i = t_{i+1} - t_i$ are Exp(λ)-distributed. Having a nonstationary Poisson process we would like to identify parts of the spike train where a constant firing rate can be assumed. In the following these parts will be called rate sections so that a rate section is defined as a part of the spike train with constant intensity.

1.3.2 The sample data set

The data to which the theory is applied are single unit recordings from spontaneously active dopaminergic neurons in the substantia nigra of mice. Each group consists of wild type mice and mice in which an ionchannel, K-ATP channel, has been tourned off (knock-out mice). In addition, it will be distinguished between calbindin-positive and calbindin-negative neurons. Calbindin is a calcium-binding protein which can be used as a marker protein in subgroups of dopaminergic neurons. Its functions, especially the contribution to the firing pattern by changes in the calbindin concentration, are not

fully understood yet. But, it has been shown for example, that neurons which express calbindin selectively survive the cell death period in Parkinson's disease.
The data are labeled by using the following abbreviations (see Table 1.1).

Abbreviation	Meaning
Location	
sn	substantia nigra
Calbindin expression	
+	Calbindin positive
-	Calbindin negative
Gene	
ko	knock out
wt	wild type

Table 1.1: Overview of the abbreviations for the labels of the data.

This dataset was recorded for previous studies and provided by Julia Schiemann and Prof. Dr. Jochen Roeper from the Institute for Neurophysiology in Frankfurt am Main. In the majority of cases the spike trains are about 720 seconds long. Moreover, it was observed that the average firing rates lie between 0.8 and 8. As an example figure 1.4 presents the occurrence times of two spike trains. It can be seen that they show different irregularities of firing: the firing pattern in "sn- ko5" seems to be more regular as the ISIs differ not so much like it can be observed in "sn+ ko1". With regard to the average intensities in the time interval $[0, 75s]$ it is $\frac{N(0,75)}{75} = 4.84$ ("sn- ko5") and $\frac{N(0,75)}{75} = 3.24$ ("sn+ ko1").

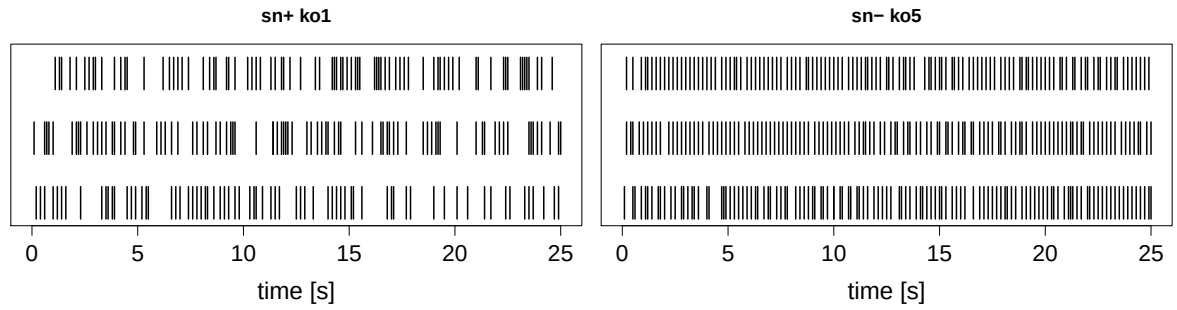

Figure 1.4: Example of two spike trains which show different irregularities of firing. One row presents the occurrence times of spikes in a time window of $25s$ e.g. first row $\hat{=} [0, 25s]$, ..., third row $\hat{=} (50s, 75s]$.

2 Detection of rate changes by means of time-dependent step filters

This chapter presents an easily applicable statistical method for the detection of rate changes in spike trains. It has been developed on the basis of earlier graphical approaches which will be described in chapter 3 for reasons of completeness.

2.1 Developing a test

Consider a spike train modeled by a stationary Poisson process with constant rate parameter λ. Dividing the spike train into intervals of length h the expected number of spikes in one interval is λh with standard deviation $\sqrt{\lambda h}$. So comparing the number of spikes in two nonoverlapping intervals gives that the expected difference is zero with standard deviation $\sqrt{2\lambda h}$.
Now, think of a spike train of length T modeled by a nonstationary Poisson process where the ISIs in the first half of the spike train are $\text{Exp}(\lambda_1)$- and in the second half $\text{Exp}(\lambda_2)$-distributed which means that there is a rate change at time $(T/2)$. Comparing the number of spikes in two intervals from the same part of the spike train, their difference will behave like those in the stationary case. But when comparing spike counts in intervals from the first with those from the second part, then the expected difference is $(\lambda_1 - \lambda_2) \cdot h$ with standard deviation $\sqrt{(\lambda_1 + \lambda_2) \cdot h}$.
Upon these observations a method for the detection of rate changes is developed, which is termed the Step-Filter-Test (SF-Test).

2.1.1 Test statistic

We divide a Poisson process into intervals with length $h[s]$ in the following way: for every time point $t \in \{h, h+1, \ldots, T-h+1, T-h\}$ the two time intervals $[t-h, t]$ (left window) and $(t, t+h]$ (right window) are disposed and the number of spikes, $N_1 =$

$N(t-h,h)$ and $N_2 = N(h,h+t)$, are determined (see figure 2.1). The left and right interval are nonoverlapping so that N_1 and N_2 are independent.

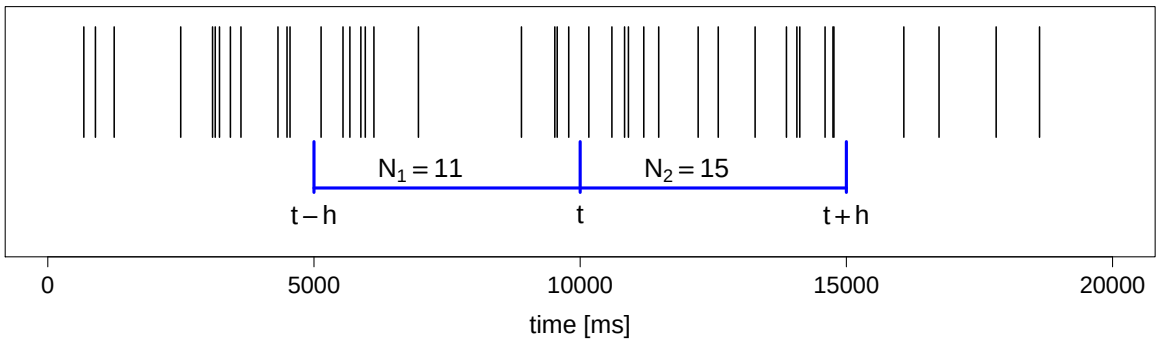

Figure 2.1: Schematical presentation of extracting two adjacent intervals $[t-h,t]$ and $(t,t+h]$ out of the spike train and counting the spikes in there (here: $t = 10s$, $h = 5s$).

In order to compare the number of spikes in the left and right window we substract N_1 from N_2 and normalise it with the square root of the estimated variance of spikes in $[t-h,t+h]$ under the assumption that the number of spikes in that time interval is Pois$(2h\hat{\lambda})$-distributed with $\hat{\lambda} = \dfrac{N(t-h,t+h)}{2h}$, the mean firing rate in $[t-h,t+h]$. So for a fixed window size h we compute for every time point $t \in \{h, h+1, \ldots, T-h+1, T-h\}$ the value

$$D_{h,t} = \frac{(N_1 - N_2)}{\sqrt{2h\hat{\lambda}}}.$$

This procedure can be done for different window sizes h, whereas we will see later on that only a few different choices of h are needed for determining if the number of spikes differ more from each other than it would be expected under the assumption that N_1 and N_2 are from the same distribution.
To get a more compact presentation of $D_{h,t}$ it is transformed by replacing $\hat{\lambda}$ in the denominator by

$$\frac{N(t-h,t+h)}{2h} = \frac{(N_1+N_2)}{2h}$$

so we come out with

$$\begin{aligned} D_{h,t} &= \frac{(N_1 - N_2)}{\sqrt{2h \cdot \frac{(N_1+N_2)}{2h}}} \\ &= \frac{(N_1 - N_2)}{\sqrt{(N_1+N_2)}} \end{aligned} \tag{2.1}$$

In the example in figure 2.1 we would get for $h = 5s$ and $t = 10s$

$$D_{5,10} = \frac{(11 - 15)}{\sqrt{11 + 15}} \approx -0.79$$

and holding $h = 5s$ fixed $D_{5,t}$ can be computed for varying $t[s]$, here: $t = 5s, 6s, \ldots, 34s, 35s$ (see figure 2.2).

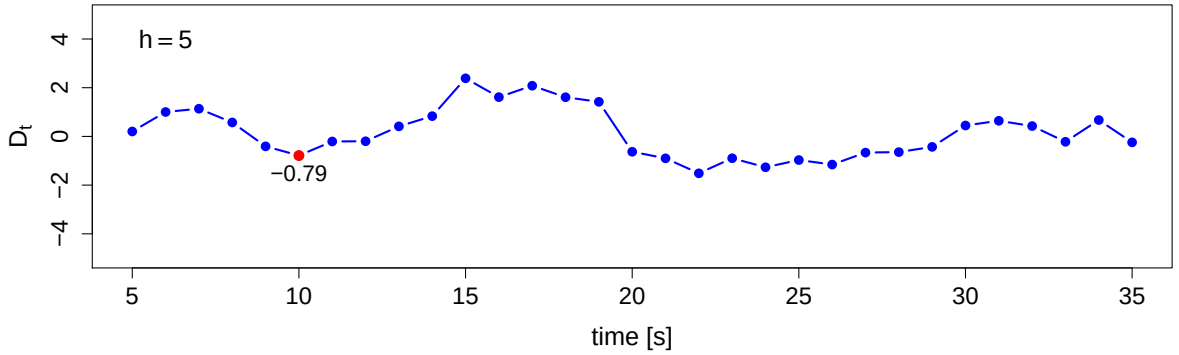

Figure 2.2: Test statistic $D_{5,t}$ for $t = 5s, 6s, \ldots, 34s, 35s$. The red point marks $D_{5,10}$.

In order to be able to evaluate the observed difference between N_1 and N_2 respectively to make statements about $D_{h,t}$ in comparison to what has been expected under the null hypothesis, a decision rule has to be developed.
First of all it is necessary to substantiate the null hypothesis H_0 and the alternative hypothesis H_1. We assume $N_1 \sim \text{Pois}(\lambda_1 \text{h})$ and $N_2 \sim \text{Pois}(\lambda_2 \text{h})$, with

$$H_0\colon\ \lambda_1 = \lambda_2 \quad \text{and} \quad H_1\colon\ \lambda_1 \neq \lambda_2.$$

The next step will be to establish a decision rule which allows to decide whether or not to reject the null hypothesis in favor of the alternative. Comparing the test-statistic (equation 2.1) to the critical value K the decision rule is to reject H_0 if $|D_{h,t}| > K$. In order to define K we need to know how $D_{h,t}$ is distributed under the null hypothesis. This means that it has to be examined what happens when applying the Step-Filter-Test to stationary Poisson processes (see figure 2.3).
First of all the distribution of $D_{h,t}$ under H_0 can be determined by drawing two random numbers p_1 and p_2 from a Pois(λh)-distribution several times and compute every time $D_{h,t} = \frac{(p_1 - p_2)}{\sqrt{(p_1 + p_2)}}$. In doing so about 10000 times we get an approximation of the distribution of $D_{h,t}$ under H_0 (see figure 2.3).
It is by definition symmetrical around zero with standard deviation 1 independent of λ respectively h. Furthermore it is $|Q_{0.005}| = Q_{0.995} = 2.6$, the 0.5%- respectively 99.5%-quantile, so that only in one of 100 cases it can be expected to observe $|D_{h,t}| \geq 2.6$. However, having a recording time $T = 720s$ and a window width $h = 10s$ we get 700

values for $|D_{10,t}|$ so that it can be expected that seven of them will be above 2.6 given that they were all independent.

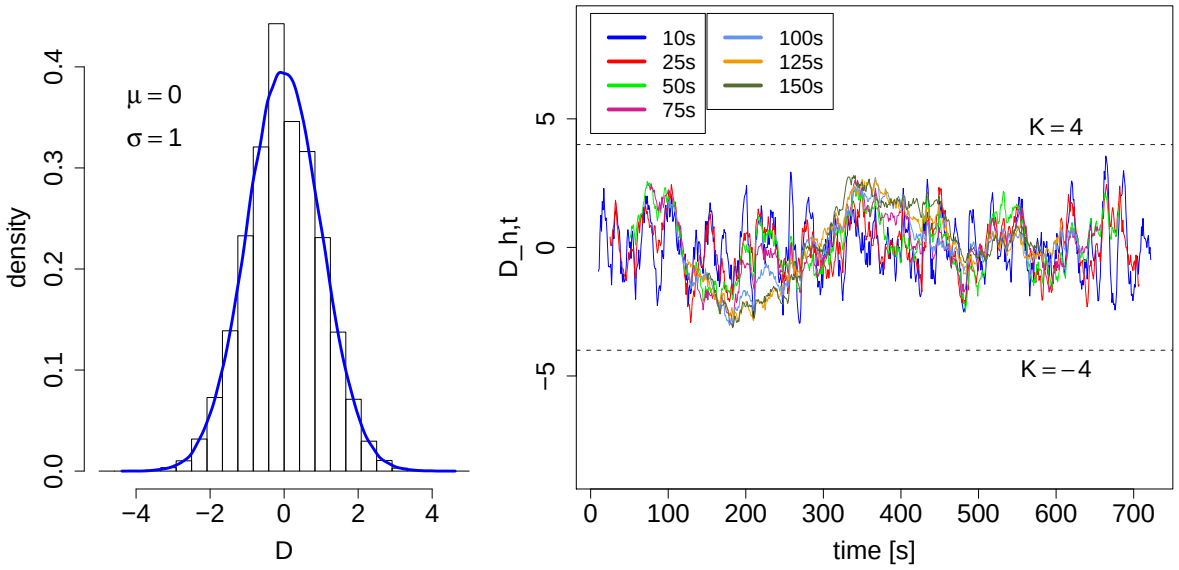

Figure 2.3: Left: Distribution of D under H_0. Right: Resulting lines when applying the Step-Filter-Test to a stationary Poisson process with h successively taken as $10s, 25s, 50s, 75s, 100s, 125s, 150s$ (see legend). The dashed lines mark the range for which the null model is not rejected (see text passage below).

Indeed, this boundary does not take into account that the results for $D_{10,t}$ are not independent $\forall\ t$ because of taking overlapping intervals. Moreover, applying the Step-Filter-Test to the spike train, different window sizes are taken so that one gets all in all more than 700 values for $D_{h,t}$ which are also interdependent. As a result, the Step-Filter-Test would often find rate changes in a stationary Poisson process (false positive results).

We need a boundary so that in 100 simulated stationary Poisson processes of T seconds with constant rate λ only in k cases it can be observed that $|D_{h,t}| > K$ whereby h is chosen successively as $10s, 25s, 50s, 75s, 100s, 125s, 150s$. Here we choose $k = 1$ so we get a strict boundary in order to exclude many false positive results or in other words results which are erroneously positive when H_0 is true.

In order to find this limit, the proposed test is applied to 1000 stationary Poisson processes with constant rate parameter λ where the computation of $D_{h,t}$ is done for $t = h, h+1, \ldots, (T-h)\ \forall\ h \in \{10s, 25s, 50s, 75s, 100s, 125s, 150s\}$. The critical value K is chosen so that only in 10 of 1000 processes $D_{h,t}$ falls outside of $[-4, 4]$. In doing so we get $K = 4$ as approximate 99%-confidence limit (see figure 2.3).

2.1.2 Asymptotic expectation and variance

In order to determine the asymptotic expectation and variance of $D_{h,t}$ the δ-method is used which is a method for deriving an approximate probability distribution for a function of random variables based on Taylor series expansions. In its essence, the δ-method expands the given function up to the second term about its mean and then takes the variance or the expectation.
For example, in the one-dimensional case if one wants to approximate the expectation and the variance of f(X) where X is a random variable with $E[X] = \mu$, $\mathrm{Var}[X] = \sigma^2$ and f satisfies the property that $f'(\mu)$ exists and is non-zero valued, one can try the following steps:
1. Taylor series expansion of f(X) about μ:

$$f(X) = f(\mu) + (X - \mu)\frac{df}{dX}\Big|_{\mu} + ...$$

2. Dropping the higher order terms to give the approximation:

$$f(X) \approx f(\mu) + (X - \mu)\frac{df}{dX}\Big|_{\mu}$$

3. Taking the expectation respectively the variance of both sides yields:

$$\begin{aligned} E(f(X)) &\approx f(\mu) \\ \mathrm{Var}(f(X)) &\approx \mathrm{Var}(X) \cdot \left[\frac{df}{dX}\Big|_{\mu}\right]^2 \end{aligned}$$

Two-dimensional δ-method

The idea from above can be expanded to vector-valued functions of random vectors. Here we restrict ourselves to the two-dimensional case which we need for the computation of the variance and the expectation of $D_{h,t}$.
Suppose we have random variables X_1 and X_2 which are independent. A taylor series expansion of $f(X_1, X_2)$ about the value $\mu = (\mu_1, \mu_2)$ is given by:

$$\begin{aligned} f(X_1, X_2) &= f(\mu_1, \mu_2) + \frac{\partial f(X_1, X_2)}{\partial X_1}\Big|_{(\mu_1,\mu_2)}(X_1 - \mu_1) \\ &+ \frac{\partial f(X_1, X_2)}{\partial X_2}\Big|_{(\mu_1,\mu_2)}(X_2 - \mu_2) + \underbrace{o(||X - \mu||)}_{\text{higher order terms}} \end{aligned} \tag{2.2}$$

Dropping the higher order terms in equation 2.2 one gets an approximation of $f(X_1, X_2)$. As in the one-dimensional case the expectation can be approximated by:

$$E[f(X_1, X_2)] \approx f(\mu_1, \mu_2)$$

and the variance by:

$$\begin{aligned}\mathrm{Var}[f(X_1,X_2)] &\approx \mathrm{Var}[f(\mu_1,\mu_2)] + \frac{\partial f(X_1,X_2)}{\partial X_1}\Big|_{(\mu_1,\mu_2)}(X_1-\mu_1) \\ &+ \frac{\partial f(X_1,X_2)}{\partial X_2}\Big|_{(\mu_1,\mu_2)}(X_2-\mu_2) \\ &= \left(\frac{\partial f(X_1,X_2)}{\partial X_1}\Big|_{(\mu_1,\mu_2)}\right)^2 \mathrm{Var}[X_1] \\ &\quad + \left(\frac{\partial f(X_1,X_2)}{\partial X_2}\Big|_{(\mu_1,\mu_2)}\right)^2 \mathrm{Var}[X_2] \end{aligned} \tag{2.3}$$

Note that X_1 and X_2 are independent which means that terms which include the covariance of X_1 and X_2 are zero and hence omitted in the computation.

Now the δ-method is applied to our given problem: the determination of the expectation and the variance of $D_{h,t} = \dfrac{(N_1 - N_2)}{\sqrt{(N_1+N_2)}}$.

Let N be the two-dimensional random vector $N = (N_1, N_2)$ where N_1 and N_2 are independent with $\mathrm{Var}[N_1] = \lambda_1 h$, $\mathrm{Var}[N_2] = \lambda_2 h$ and $\mathrm{Cov}(N_1, N_2) = 0$.
Let $\mu = (\mu_1, \mu_2)$ be the two-dimensional vector parameter with $\mu_1 = E[N_1] = \lambda_1 h$ and $\mu_2 = E[N_2] = \lambda_2 h$.
Note that N_i is a poisson distributed random variable with parameter $\lambda_i h$. Thus, for sufficiently large values of h N_i has asymptotic normal distribution with expectation $\lambda_i h$ and variance $\lambda_i h$.

We define $f(x,y) = \dfrac{(x-y)}{\sqrt{x+y}}$ with

$$\begin{aligned}\frac{\partial f}{\partial x} &= \frac{1}{\sqrt{x+y}} + (x-y)\cdot\left(\frac{-1}{2}\right)\cdot(x+y)^{\frac{-3}{2}} \\ \frac{\partial f}{\partial y} &= \frac{-1}{\sqrt{x+y}} + (x-y)\cdot\left(\frac{-1}{2}\right)\cdot(x+y)^{\frac{-3}{2}} \ .\end{aligned}$$

Then the expectation of $D_{h,t} = f(N_1, N_2)$ can be approximated by:

$$\begin{aligned} E\left[f(N_1,N_2)\right] &\approx f(\mu_1,\mu_2) \\ &= \frac{(\mu_1-\mu_2)}{\sqrt{\mu_1+\mu_2}} \\ &= \frac{(\lambda_1-\lambda_2)}{\sqrt{\lambda_1+\lambda_2}}\cdot\sqrt{h} \end{aligned} \tag{2.4}$$

and the variance of $D_{h,t} = f(N_1, N_2)$ by:

$$\begin{aligned} \mathrm{Var}\left[f(N_1,N_2)\right] &= \mathrm{Var}\left[\frac{(N_1-N_2)}{\sqrt{N_1+N_2}}\right] \\ &\approx 1-\frac{3}{4}\frac{(\lambda_1-\lambda_2)^2}{(\lambda_1+\lambda_2)^2} \end{aligned} \tag{2.5}$$

$\Rightarrow f(N_1, N_2) = D_{h,t}$ has asymptotic normal distribution with asymptotic expectation μ

$$\mu = \frac{(\lambda_1-\lambda_2)}{\sqrt{\lambda_1+\lambda_2}} \cdot \sqrt{h}$$

and asymptotic variance σ^2

$$\sigma^2 = 1-\frac{3}{4}\frac{(\lambda_1-\lambda_2)^2}{(\lambda_1+\lambda_2)^2}\ .$$

Proof of equation 2.5

$$\begin{aligned} \mathrm{Var}\left[f(N_1,N_2)\right] &\approx \left(\frac{\partial f(N_1,N_2)}{\partial N_1}\Big|_{(\mu_1,\mu_2)}\right)^2 \mathrm{Var}[N_1] + \left(\frac{\partial f(N_1,N_2)}{\partial Y}\Big|_{(\mu_1,\mu_2)}\right)^2 \mathrm{Var}[N_2] \\ &= \left[\frac{1}{\sqrt{E[N_1]+E[N_2]}} + \frac{(E[N_1]-E[N_2])}{(E[N_1]+E[N_2])^{\frac{3}{2}}}\cdot\left(\frac{-1}{2}\right)\right]^2 \cdot \mathrm{Var}[N_1] \\ &\quad + \left[\frac{-1}{\sqrt{E[N_1]+E[N_2]}} + \frac{(E[N_1]-E[N_2])}{(E[N_1]+E[N_2])^{\frac{3}{2}}}\cdot\left(\frac{-1}{2}\right)\right]^2 \cdot \mathrm{Var}[N_2] \\ &= \frac{\mathrm{Var}[N_1]}{(E[N_1]+E[N_2])}\cdot\left[1-\frac{(E[N_1]-E[N_2])}{2(E[N_1]+E[N_2])}\right]^2 \\ &\quad + \frac{\mathrm{Var}[N_2]}{(E[N_1]+E[N_2])}\cdot\left[-1-\frac{(E[N_1]-E[N_2])}{2(E[N_1]+E[N_2])}\right]^2 \\ &= \frac{\lambda_1 h}{(\lambda_1+\lambda_2)h}\left(1+\frac{(\lambda_1-\lambda_2)h}{2(\lambda_1+\lambda_2)h}\right)^2 + \frac{\lambda_2 h}{(\lambda_1+\lambda_2)h}\left(-1-\frac{(\lambda_1-\lambda_2)h}{2(\lambda_1+\lambda_2)h}\right)^2 \\ &= \frac{\lambda_1}{(\lambda_1+\lambda_2)}\left(1-\frac{(\lambda_1-\lambda_2)}{(\lambda_1+\lambda_2)}+\frac{1}{4}\frac{(\lambda_1-\lambda_2)^2}{(\lambda_1+\lambda_2)^2}\right) \\ &\quad + \frac{\lambda_2}{(\lambda_1+\lambda_2)}\left(1+\frac{(\lambda_1-\lambda_2)}{(\lambda_1+\lambda_2)}+\frac{1}{4}\frac{(\lambda_1-\lambda_2)^2}{(\lambda_1+\lambda_2)^2}\right) \\ &= 1+\frac{(\lambda_2-\lambda_1)(\lambda_1-\lambda_2)}{(\lambda_1+\lambda_2)^2}+\frac{1}{4}\frac{(\lambda_1-\lambda_2)^2(\lambda_1+\lambda_2)}{(\lambda_1+\lambda_2)^3} \\ &= 1-\frac{(\lambda_1-\lambda_2)^2}{(\lambda_1+\lambda_2)^2}+\frac{1}{4}\frac{(\lambda_1-\lambda_2)^2}{(\lambda_1+\lambda_2)^2} \\ &= 1-\frac{3}{4}\frac{(\lambda_1-\lambda_2)^2}{(\lambda_1+\lambda_2)^2} \end{aligned}$$

Properties of μ and σ^2

As we already know, it can be affirmed that for every stationary Poisson process $D_{h,t}$ has expectation 0 and variance 1 independent of λ ($\lambda_1 = \lambda_2$) and the choice of the window size.

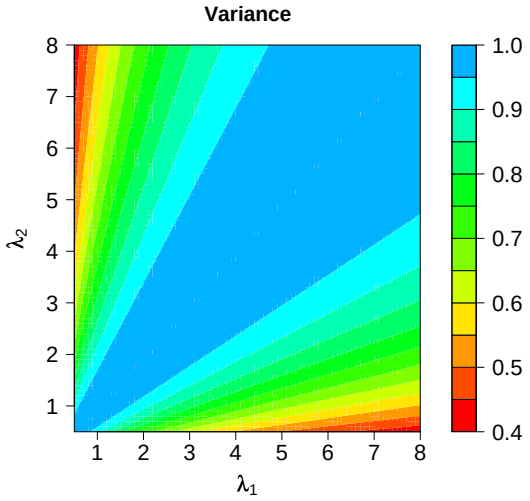

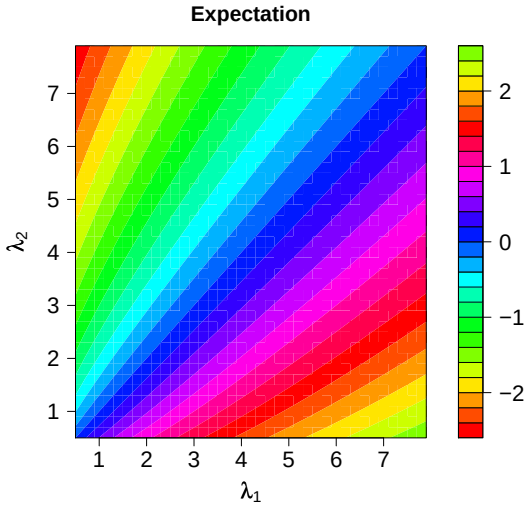

Apart from that σ^2 only depends on λ_1 and λ_2. It is independent of the window size h and takes values between 0 and 1. It is 1 for $\lambda_1 = \lambda_2$ and smaller 1 if $\lambda_1 \neq \lambda_2$ whereas the variance is nearer to 1 the greater λ_1 and λ_2 are and/or the smaller the distance between the two rates. We can restrict ourselves to $\lambda_i \leq 8$ in accordance with the intensities which have been observed in the data. It follows that $0.4 < \sigma^2 \leq 1$.

μ also depends on h but with regard to $E[D_{1,t}] \approx \frac{(\lambda_1 - \lambda_2)}{\sqrt{\lambda_1 + \lambda_2}}$ ($h = 1$ fixed) it can be seen what changes for different choices of λ_1 and λ_2: for $\lambda_i \leq 8$ we have $-2.6 \leq E[D_{1,t}] \leq 2.6$. Obviously, the expectation is nearer to 0 the smaller the distance between the two rates and/or the greater λ_1 and λ_2 are.

Knowing these properties the test power will now be evaluated.

2.1.3 Evaluation of the test power

Given $\lambda_1 \neq \lambda_2$ the probability of detecting the rate change, i.e. the probability that $D_{h,t}$ falls outside of $[-4, 4]$ under H_1, for different pairs of λ_1 and λ_2 dependent on the window size h is computed. Therefore it is assumed that for every choice of h the length of the rate sections equals h so that h is also the time point of the rate change and the two time intervals, $[0, h]$ and $(h, 2h]$, comprise the whole rate section each. As a consequence, h is always chosen as the optimal interval length for finding the rate change.

W.l.o.g. we investigate the case $\lambda_1 > \lambda_2$ so that $E[f(N_1, N_2)] > 0$.
Think of a spike train modeled by a nonstationary Poisson process with step rate function $r(t)$ where the ISIs in $[0, h]$ are Exp(λ_1)- and in $(h, 2h]$ Exp(λ_2)-distributed with $\lambda_1 > \lambda_2$. We want to determine the probability of $D_{h,h}$ (here $t = h$) lying above $K = 4$ for different window width h (= length of the rate sections) so that H_0 is rejected in favour of H_1. Hence:

$$\begin{aligned} P(D_{h,h} > 4) &= P\left(\frac{(N_1 - N_2)}{\sqrt{N_1 + N_2}} > 4\right) \\ &\approx 1 - \Phi\left(\frac{4 - \mu}{\sigma}\right) \end{aligned} \tag{2.6}$$

with $\mu = \dfrac{(\lambda_1 - \lambda_2)}{\sqrt{\lambda_1 + \lambda_2}} \cdot \sqrt{h}$ and $\sigma^2 = 1 - \dfrac{3}{4}\dfrac{(\lambda_1 - \lambda_2)^2}{(\lambda_1 + \lambda_2)^2}$ (see equation 2.4 and 2.5)

where $\Phi(z)$ is the cumulative distribution function of the standard normal distribution:

$$\Phi(z) = \frac{1}{\sqrt{2\pi}} \int_{-\infty}^{z} e^{-x^2/2} dx \ .$$

For the computation of the probability it has to be considered that $D_{h,t}$ has asymptotic normal distribution. Simulations have shown that for $h > 40s$ the results are very exact for $0.5 < \lambda_i < 8$. With respect to $h < 40s$ the error is smaller 0.02 for $\lambda_i > 2$ (see figure 2.4).

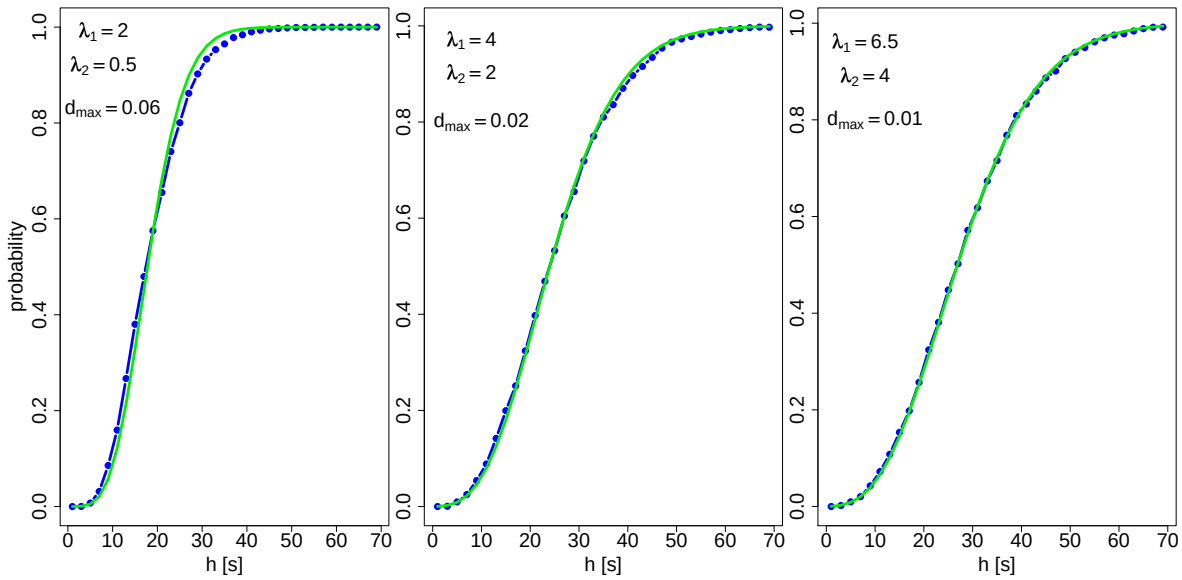

Figure 2.4: Comparison of the asymptotic test power (green line) and the test power determined in simulations (blue line) for different rate pairs. The maximal error is marked by $d_{max}\hat{=}$ maximal distance between the lines.

The next examples illustrate the test power further. If we hold $\lambda_1 = 5$ fixed and vary λ_2 so that the difference between λ_1 and λ_2 gets continuously smaller then it can be

seen that for a smaller distance the rate sections have to be longer respectively h has to be greater in order to find the rate change with a high probability (see figure 2.5).

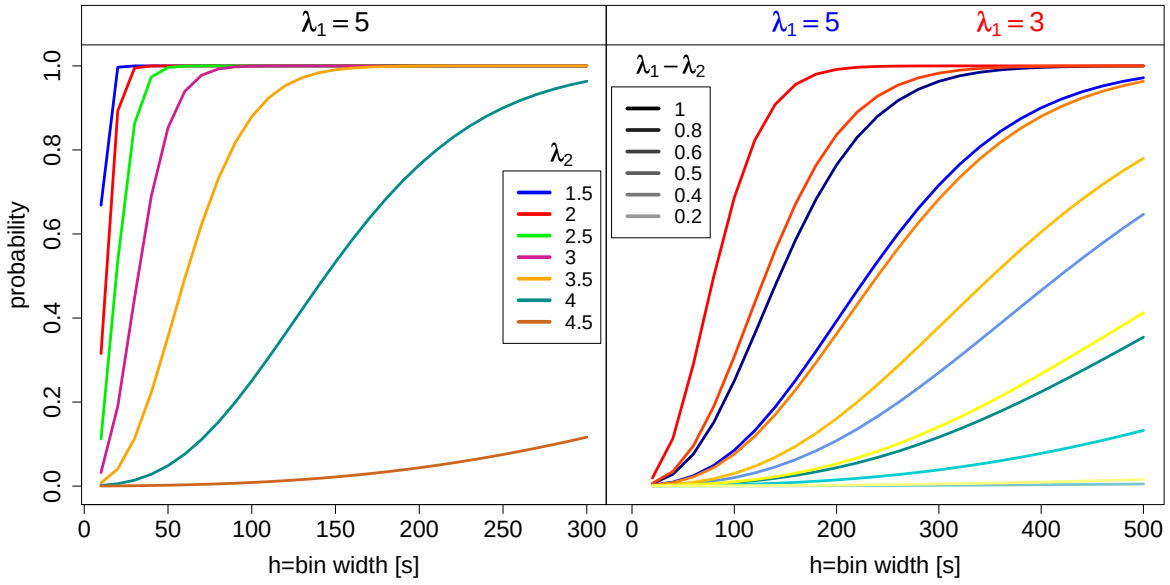

Figure 2.5: Probability of finding rate changes for different λ_i and window width h (h equals the length of one rate section).

This can be traced back to the fact that σ^2 is nearer to 1 and μ nearer to 0 (for $h = 1$) the smaller the difference between the two rates. In order to reduce this declaration to one value the expectation in relation to the standard deviation is taken, which will be called $R(\lambda_1, \lambda_2)$ in the following,

$$R(\lambda_1, \lambda_2) = \frac{\mu}{\sigma} = -R(\lambda_2, \lambda_1)$$

so that we have for a stationary Poisson process $R(\lambda, \lambda) = 0$. Coming back to the example from above one gets that the smaller the difference between the two rates the smaller the value for $R(\lambda_1, \lambda_2)$ (see figure 2.6).

For $|\lambda_1 - \lambda_2| < \epsilon$ with $0 < \epsilon < 1$ it seems unlikely that the rate change will be detected unless the rate sections are long (see figure 2.5). In addition, comparing the probability curves of $\lambda_1 = 3$ and $\lambda_1 = 5$ for $(\lambda_1 - \lambda_2) \in \{1, 0.8, 0.6, 0.5, 0.4, 0.2\}$ it gets clear that in the second case ($\lambda_1 = 5$) h has to be greater for having a high probability of finding the rate change. Note that this statement can be extended to $|\lambda_1 - \lambda_2| > 1$. With respect to the expectation of $D_{1,t}$ in relation to the standard deviation one gets that $R(3, \lambda_2) > R(5, \lambda_2) \quad \forall \quad \lambda_2$ (see figure 2.6).
To sum up, the test power i.e. the probability of finding a rate change under H_1 depends on the one hand on the length of the rate sections i.e. on the window width h. On the other hand the difference between λ_1 and λ_2 and the hight of the rates themselves

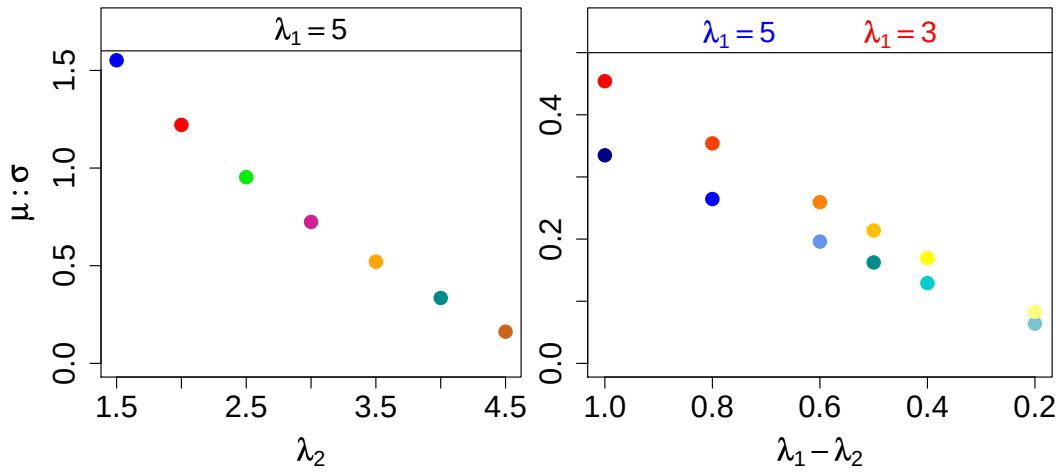

Figure 2.6: Expectation of $D_{1,t}$ in relation to its standard deviation: $R(\lambda_1, \lambda_2)$. The coloured points mark those rate combinations which have been investigated above (see figure 2.5).

influence the test power: it could be learned that for a given h the smaller $|\lambda_1 - \lambda_2| = \epsilon$ and the larger the rates for a given ϵ the smaller the test power. This interrelation can be combined in one value $R(\lambda_1, \lambda_2)$ the relation between the expectation and the standard deviation of $D_{1,t}$. Comparing $R(\lambda_1, \lambda_2)$ for different rate pairs (λ_1, λ_2) one can conclude that for a given h the larger $|R(\lambda_1, \lambda_2)|$ the larger the test power.

Identification of h for a test power of 80%

In order to determine how long the rate sections must be at least so that in 80 out of 100 cases the rate change will be found, only the case

$$\lambda_1 > \lambda_2 \Rightarrow \mu > 0$$

has to be examined for symmetry reasons: $P(D_{h,t} > 4) = P(D_{h,t} < -4)$
Having the inequality

$$P(D_{h,t} > 4) \approx 1 - \Phi\left(\frac{4-\mu}{\sigma}\right) = 0.8$$

we replace μ by $\frac{(\lambda_1 - \lambda_2)}{\sqrt{\lambda_1 + \lambda_2}} \cdot \sqrt{h}$ and then solve the inequality for h yielding

$$\begin{aligned} P(D_{h,t} > 4) &= 0.8 \\ 1 - \Phi\left(\frac{4-\mu}{\sigma}\right) &\approx 0.8 \end{aligned}$$

$$\begin{aligned} \mu &\approx 0.842 \cdot \sigma + 4 \\ \frac{(\lambda_1 - \lambda_2)}{\sqrt{\lambda_1 + \lambda_2}} \cdot \sqrt{h} &\approx 0.842 \cdot \sigma + 4 \\ h &\approx (0.842 \cdot \sigma + 4)^2 \cdot \frac{(\lambda_1 + \lambda_2)}{(\lambda_1 - \lambda_2)^2} \end{aligned}$$

with $Q_{0.2}$, the 0.2%-quantile of the standard normal distribution, approximated by 0.842. For example, with $\lambda_1 = 5$ and $\lambda_2 = 4$ (or vice verca) it is: $h = 210.5$.

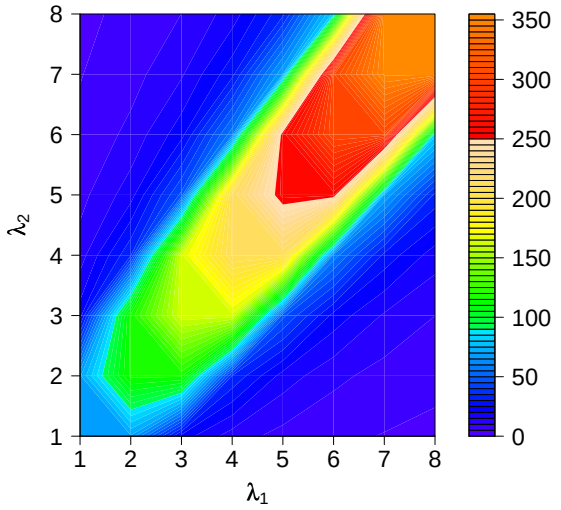

The figure on the left shows for different combinations of λ_1 and λ_2 with $\lambda_i \in \{1, 2, \ldots, 8\}$ and $\lambda_1 \neq \lambda_2$, how large h must approximately be in order to have $P(D_{h,t} > 4) = 0.8$ respectively $P(D_{h,t} < -4) = 0.8$. It can be seen that the larger λ_i for a given difference $|\lambda_1 - \lambda_2|$ or the smaller the difference $|\lambda_1 - \lambda_2|$ for a given λ_1 the bigger h has to be in order to get $P(|D_{h,t}| > 4) = 0.8$ as it has already been indicated before.

2.2 Implementation of the test

Before applying the Step-Filter-Test to simulated spike trains and to real data it is necessary to define the window sizes which will be used as well as the estimate of the change point and to determine the quality of the estimation.

2.2.1 Choice of the window size h

It is a matter of waiting up options as we have seen that rate changes only have a high probability to be found by small window sizes when the relative difference between the two rates is large enough (see figure above). However, small window sizes have the advantage that rate changes can be found more precisely because rate sections with short duration are not covered and have a chance to be recognized at all. As a consequence we decide to take seven different window sizes, namely $h = 10s, 25s, 50s, 75s, 100s, 125s, 150s$. Note that the presentation of the results

becomes quite complex when taking more values for h so that the restriction to a few window sizes is necessary.
On the one hand this choice for h allows the identification of short rate sections under the precondition that the probability to find the rate change is high enough, which means that the relative rate difference is large enough. On the other hand, if rate sections are longer and not identified by the small window sizes, for example as a consequence of $|\lambda_1 - \lambda_2| < 1$, then the rate change can be found by the higher values of h. The smallest window size was chosen as $h = 10s$ because it still allows for some rate combinations with $0.8 < \lambda_i < 8$ to find the rate difference with a high probability. The experience has shown that smaller window sizes ($h < 100s$) are more important for the reasons mentioned above and $h > 150s$ is not absolutely essential because of the strong preconditions: for rate differences which could only be found by $h > 150s$ both rate sections have to be longer than $150s$ as well which does not occur very often as the length of recording time is about $T = 720s$. In addition, for the observed firing rates in the data $0.8 < \lambda_i < 8$ it can be concluded that $h = 150s$ yields for most rate combinations an asymptotic test power of 80% (see figure 2.7).

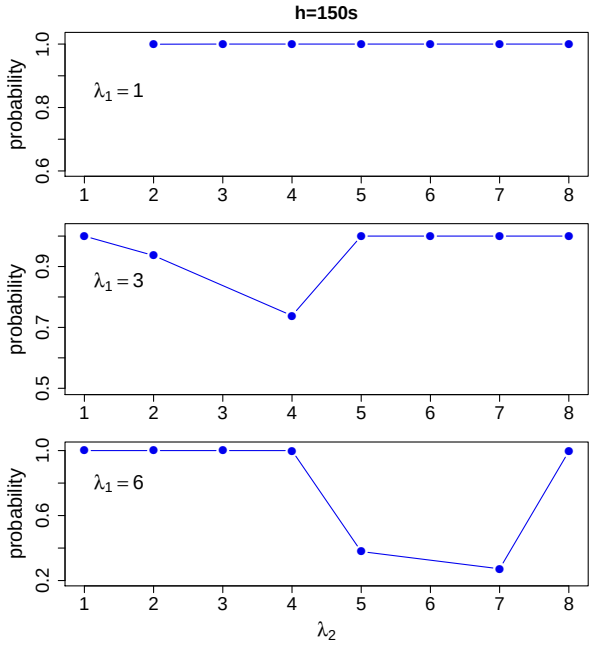

Figure 2.7: Presentation of the asymptotic test power for $h = 150s$ and $\lambda_1 = 1, 3, 6$ in combination with $\lambda_2 \in \{1, 2, \ldots, 8\} \setminus \{\lambda_1\}$.

2.2.2 Identification of the time of the rate change

Consider a spike train where in the first half of the time the ISIs are Exp(λ_1)- and in the second half Exp(λ_2)-distributed. So there is a rate change at time $t = T/2$ termed t_c

(see figure 2.8). For $h \in \{10s, 25s, 50s, 75s, 100s, 125s, 150s\}$ the distribution of N_1 and N_2 is characterized dependent on the point in time t for which $D_{h,t}$ will be evaluated:

1. for $t \leq t_c - h \;\Rightarrow$ both N_1 and N_2 are Pois$(\lambda_1 h)$-distributed
2. for $t_c - h < t < t_c \;\Rightarrow\; N_1 \sim$ Pois$(\lambda_1 h)$ and $N_2 \sim$ Pois$((\lambda_1(h-i) + \lambda_2 i))$ with $i = 1, \ldots, h-1$
3. for $t = t_c \;\Rightarrow\; N_1 \sim$ Pois$(\lambda_1 h)$ and $N_2 \sim$ Pois$(\lambda_2 h)$
4. for $t_c < t < t_c + h \;\Rightarrow\; N_1 \sim$ Pois$((\lambda_1(h-i) + \lambda_2 i))$ with $i = 1, \ldots, h-1$ and $N_2 \sim$ Pois$(\lambda_2 h)$
5. for $t \geq t_c + h \;\Rightarrow$ both N_1 and N_2 are Pois$(\lambda_2 h)$-distributed

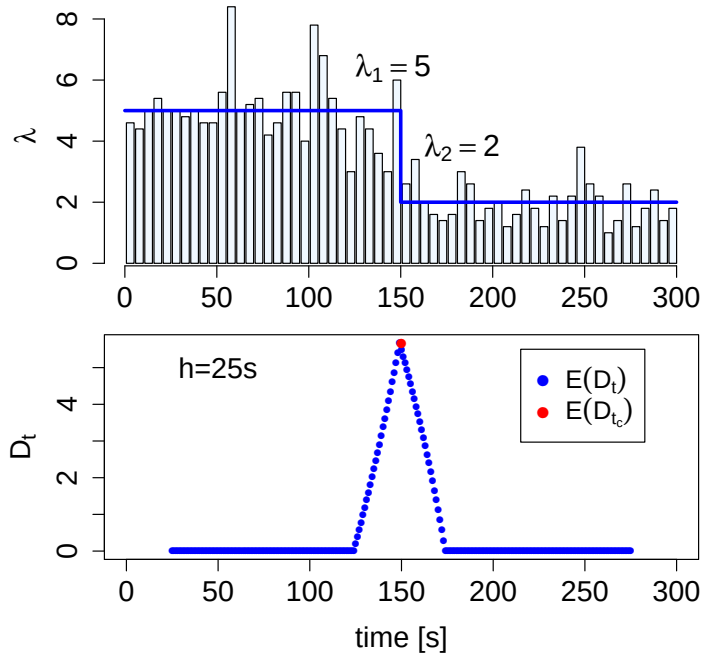

Figure 2.8: Schematical presentation of the expected values for $D_{25,t}$ in a spike train with underlying Poisson process with rate change at time $t = t_c = 150s$.

So if h is large enough we expect $|D_{h,t}| > 4$ for some t between $t_c - h$ and $t_c + h$. Furthermore the maximum of $|D_{h,t}|$ is expected to be reached for $t = t_c$ (see figure 2.8). Hence, for every window width h an estimate of the change point of the intensity, termed $\hat{t}_c^h$, can be identified as the time point t for which $|D_{h,t}| = \max_t(|D_{h,t}|)$. The average over these values could finally be taken as an estimate for t_c.

However, under the precondition that the spike train consists of more than one rate change, taking the average is only suitable if the length of the rate sections is bigger

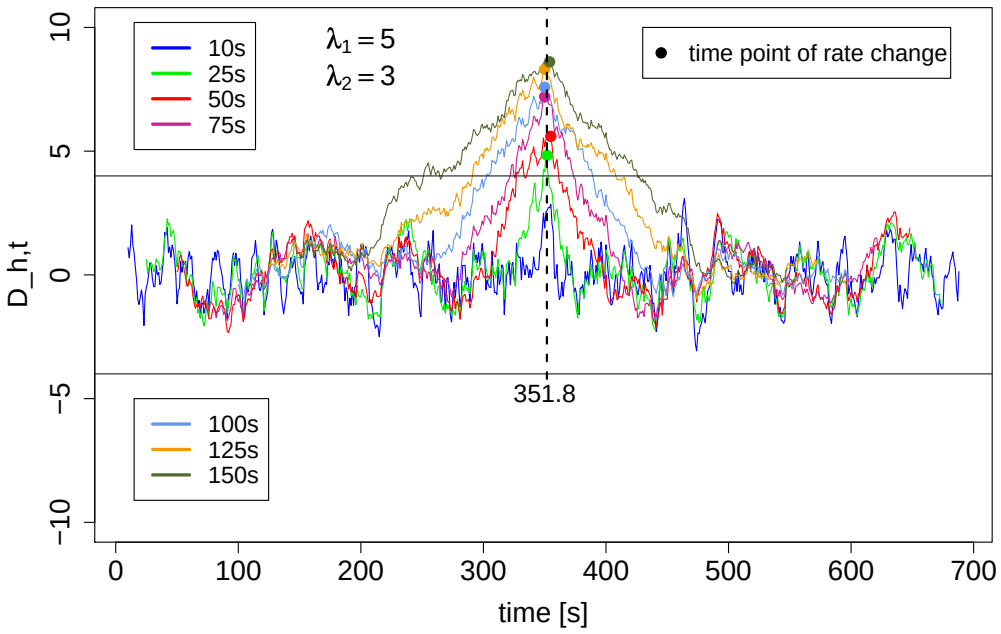

Figure 2.9: Application of the Step-Filter-Test to a spike train with underlying nonstationary Poisson process. The maxima of the curves are taken as an estimate of the time point of rate change. The dashed line marks the average over all $\hat{t}_c^h$ $(h = 10s, 25s, \ldots, 150s)$.

than h. Otherwise, one gets false information because the rate sections would be covered by larger window sizes (see figure 2.10). More precisely, the decisive time interval $[t_c - h, t_c + h]$ would include apart from t_c another rate change (see figure 2.10: t_{c_2}) or in the case of the first (last) rate change the SF-method starts with $t = h > t_c$ so the rate change would not be recognized correctly (see figure 2.10: t_{c_1}). As a consequence, we take the minimum over all h which have detected the rate change ($|D_{h,t}| > 4$ was observed), label it h^* and define the estimate of the time point of the rate change by

$$\hat{t}_c = \hat{t}_c^{h^*}.$$

Having more than one rate change we will get different sections with $|D_{h,t}| > 4$. In every section $\hat{t}_c$ will be determined with the technique described above (see figure 2.10) whereas h^* can differ from case to case. So for the ith rate change the estimate is labelled

$$\hat{t}_{c_i} = \hat{t}_{c_i}^{h_i^*}.$$

Note that the Step-Filter-Method works under the assumption that the underlying Poisson process is characterized by a step rate function. In order to define the respective sections one could assume that low and high rates alternate so that the method has to search alternately for a peak in the region above 4 and one in the region below -4.

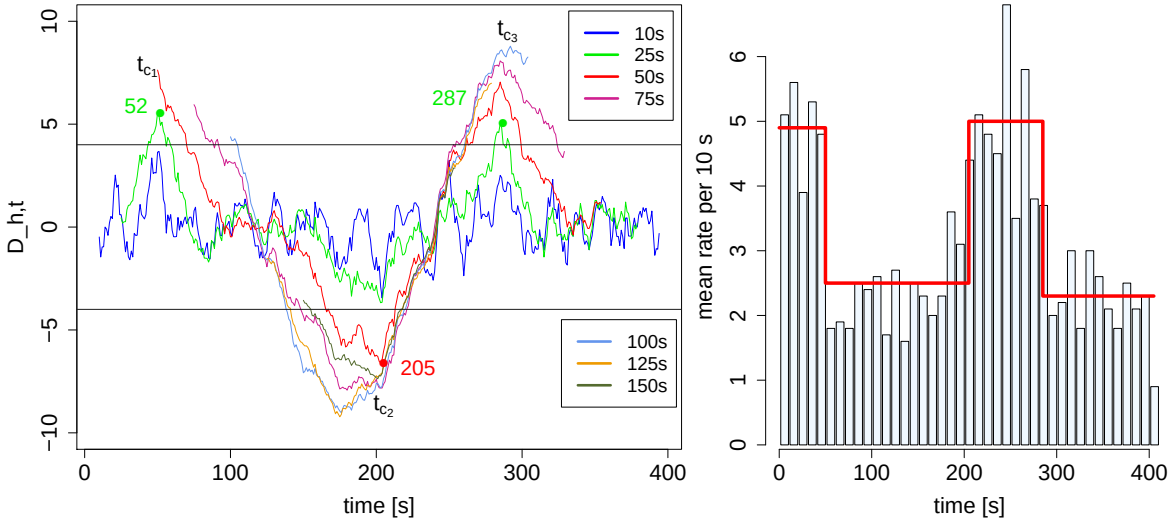

Figure 2.10: Left: Application of the Step-Filter-Test to a spike train with underlying Poisson process. The estimations of t_{c_i} identified by $\hat{t}_{c_i}^{h_i^*}$ are marked by the coloured points. Here: for the estimation of t_{c_1} and t_{c_2} the large window sizes are imprecise. Right: Average intensity in intervals of length 10s. The red line marks the true step rate function of the process.

This precondition seems to be necessary in the case that a line which has crossed the boundary falls shortly back into the interval $[-4, 4]$ by chance and then crosses the boundary again. Without the determined condition the method would identify two areas in which a change point is identified. However, a decreasing (increasing) step function would then be excluded as one observes twice in a row sections which are below (above) $K = 4$. In an effort to tackle this problem, the sections respectively the duration of $|D_{h,t}| < 4$ between two sections are defined dependent on h. As a result, it is ruled out that another change point is found by mistake as the time where $D_{h,t}$ falls back into $[-4, 4]$ is too short. But it will be possible to find decreasing (increasing) steps.

2.2.3 Precision of the identified change point

Imagine a spike train with underlying nonstationary Poisson process which can be divided into two parts with constant firing rate each. Having determined $\hat{t}_c$ we would like to know how well the time of the change has been pinpointed. This can be found out by simulating several times Poisson processes of length T where the intensity changes at a fixed time point t_c. Having determined $\hat{t}_c$ in every one of those simulations the average and the standard deviation of $\hat{t}_c$ is computed. This can be done for different combinations of λ_1 and λ_2 (see table 2.1).

λ_1	λ_2	$\lvert\lambda_1 - \lambda_2\rvert$	$R(\lambda_1, \lambda_2)$	Mean value [s]	Standard deviation [s]
5	1	4	2.0	200.21	1.49
5	2	3	1.22	200.43	2.28
5	3	2	0.73	199.48	6.42
3	1	2	1.11	200.44	2.83
6	4	2	0.64	199.86	8.63
6	3	3	1.04	200.52	3.62
7	4	3	0.93	199.78	4.64

Table 2.1: Average and standard deviation of $\hat{t}_c$ determined for different combinations of λ_1 and λ_2 in 100 simulated poisson spike trains with $T = 400s$ so that $t_c = 200s$. Only those rate combinations were examined for which the test power is 99% by $h = 150s$ at the latest.

It can be seen that for fixed $|\lambda_1 - \lambda_2|$ the larger the rates the larger the standard deviation which means that the estimate of t_c varies more. In addition, for λ_1 fixed (here $\lambda_1 = 5$) the time of the change can be more accurately pinpointed the larger the distance to λ_2. In conclusion, the estimate of the change point of the intensity is more exactly for larger values of $R(\lambda_1, \lambda_2)$ which means that the expectation of the test statistic $D_{h,t}$ in relation to its standard deviation is greater. For $R(\lambda_1, \lambda_2) < 1$ the confidence interval for the time of the change is rather wide so that one has to expect that the estimate of t_c is not very exact.

2.2.4 Application to simulations

In order to evaluate the properties of our proposed test, it is applied to nonstationary Poisson processes with different step rate functions. Here two examples will be given. The illustrations demonstrate the results of the method on the left and the average intensity in defined intervals with the true and the estimated step rate function on the right.

Figure 2.11 presents an example where the first two rate changes ($t_{c_1} = 170s$, $t_{c_2} = 195s$) were not detected i.e. H_0 was erroneously not rejected in both cases. This can be attributed to the short rate section lasting from 170s to 195s where the underlying Poisson process has intensity $\lambda_2 = 3$ with $\lambda_1 - \lambda_2 = |\lambda_2 - \lambda_3| = 1.5$ and a test power of only 10% for $h = 25s$. By contrast, the last two rate changes, $t_{c_3} = 300s$ and $t_{c_4} = 350s$, have been identified as the rate sections are longer and the differences between the rates higher. Here the test power is 99% for $h = 50s$ in both cases. The estimated change

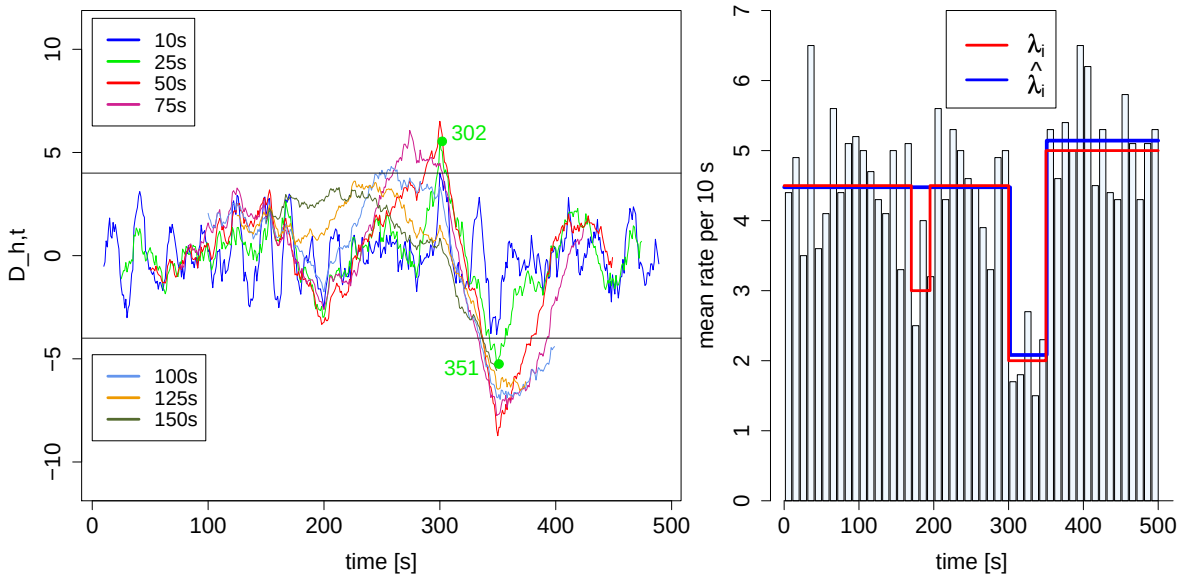

Figure 2.11: Outcome of the Step-Filter-Test and rate profile of a simulated nonstationary Poisson process. The red line indicates the true rate function and the blue line the estimated one out of the realization.

points differ from the true ones by at most 2s.

The second spike train includes seven rate changes. Six of them could have been pinpointed with $|t_{c_i} - \hat{t}_{c_i}| < 2.7$. The fourth rate change $t_{c_4} = 190s$ was not detected with a test power of only 15.6% for $h = 25s$, $\lambda_4 = 3.8$ and $\lambda_5 = 2.3$. Here we have an example of the case that it would not be appropriate if the method has to search alternately for a peak in the region above 4 and one in the region below -4: as the forth rate change was missed the lines do not cross the upper boundary in the time window $[164s, 251s]$. By defining the sections dependent on h the area around the third and fifth rate change are identified as two independent ones because the duration of $D_{h,t} < 4$ in between is long enough. So both changes, $\hat{t}_{c_3} = 164s$ and $\hat{t}_{c_5} = 251s$, could have been detected.

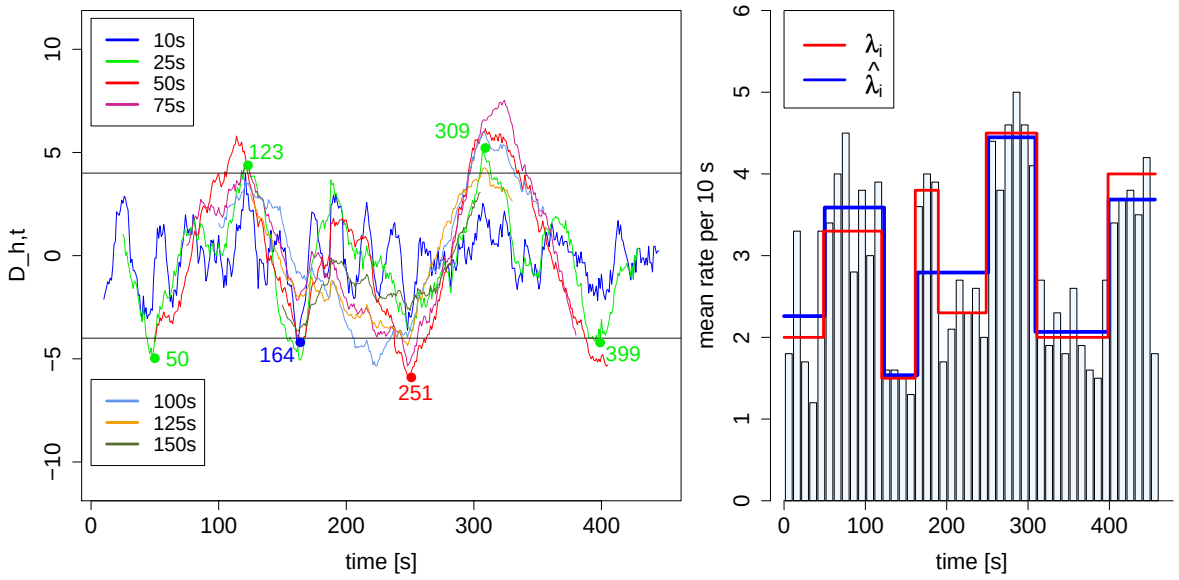

Figure 2.12: Outcome of the Step-Filter-Test and rate profile of a simulated Poisson process. The red line indicates the true rate function and the blue line the estimated one out of the realization.

2.2.5 Application to real data

In this subsection the Step-Filter-Test is applied to the data, namely spontaneous activity spike trains recorded from dopaminergic neurons in the substantia nigra of mice. In order to demonstrate the capabilities of the proposed method, a selection of examples will be presented. The data are labelled as described in table 1.1 in subsection 1.3.2. Again, the illustrations show the results of the method on the left and the average intensity in defined intervals with the estimated step rate function on the right.

1. Spike train "sn+ ko8"

The Step-Filter-Test detects three changes in the intensity, namely $\hat{t}_{c_1} = 78s$, $\hat{t}_{c_2} = 339s$ and $\hat{t}_{c_3} = 499s$, so that four sections can be separated. In each section the firing rate is estimated and the resulting rate function is illustrated in figure 2.13 on the righthand-side in form of the blue line with $\hat{\lambda}_1 = 2.91$, $\hat{\lambda}_2 = 4.49$, $\hat{\lambda}_3 = 3.01$, $\hat{\lambda}_4 = 4.20$.
For the second and third rate change $h = 100s$ is needed in order to detect the changes because the differences between the rates are at most 1.5. As the rate sections are long enough this causes no problems. For the first rate change the large window sizes cannot accurately pinpoint the change because of $\hat{t}_{c_1} < 100s$. Here, $|\hat{\lambda}_1 - \hat{\lambda}_2| = 1.6$ so that the test power for $h = 75s$ is still 85.7%.

2. Spike train "sn+ wt1"

Two rate changes are detected (see figure 2.14) yielding a short rate section of 27s with

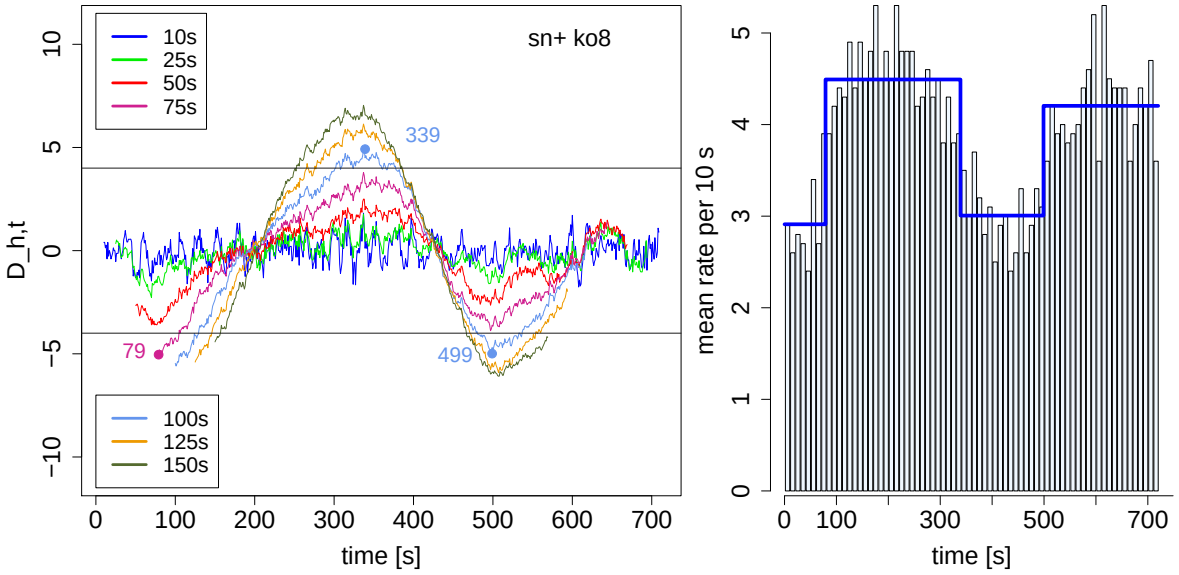

Figure 2.13: Application of the method to "sn+ ko8". The left picture shows the identified change points: 78s, 339s, 499s. The bar plot on the right presents the average intensity in intervals of length 10s. The blue line marks the estimated step rate function according to the located changes.

estimated firing rate 2.89 which is surrounded by two larger sections with estimated firing rates about 5.81 so that all window sizes with $h > 27s$ perform worse. As the difference between the rates is nearly 3 one has a test power of 85.0% for $h = 25s$. Note that for $h = 10s$ the test power would only be 17.1% for the same rates.

3. Spike train "sn+ wt4"

The result of the application of the Step-Filter-Method provides five time points of rate change so that the spike train can be separated into six sections (see figure 2.15). All changes have been detected by $h = 50s$ respectively $h = 25s$ which can be attributed to low rates ($0.8 < \hat{\lambda}_i < 4.3$) with sufficiently large differences between the rates. In the area of the second rate change ($327s$) the small window sizes indicate that there seems to be a decreasing intensity: for example the red lines falls back into $[-4, 4]$ after the time point 327s, goes down and then goes up again but fails to cross the boundary $K = 4$.

4. Spike train "sn- ko2"

The analysis detects one rate change (see figure 2.16): $\hat{t}_{c_1} = 364s$. So one gets two rate sections with intensities $\hat{\lambda}_1 = 7.64$ and $\hat{\lambda}_2 = 6.03$ with $\hat{\lambda}_1 - \hat{\lambda}_2 = 1.61$. As the intensities are higher the test power will only be bigger than 80% for $h \geq 125s$. In addition, the combination of high rates and small differences between the rates results in a greater standard deviation concerning the estimation of the change point (see table 2.1).

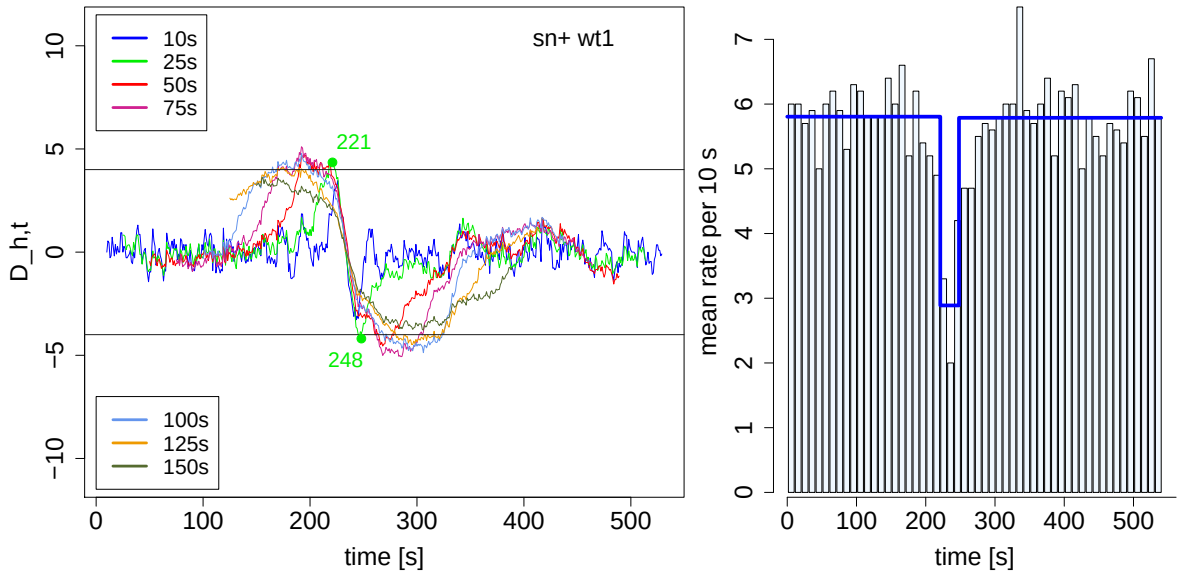

Figure 2.14: Application of the method to "sn+ wt1". The left picture shows the identified change points: 221s, 248s. The bar plot on the right presents the average intensity in intervals of length 10s. The blue line marks the estimated step rate function according to the located changes.

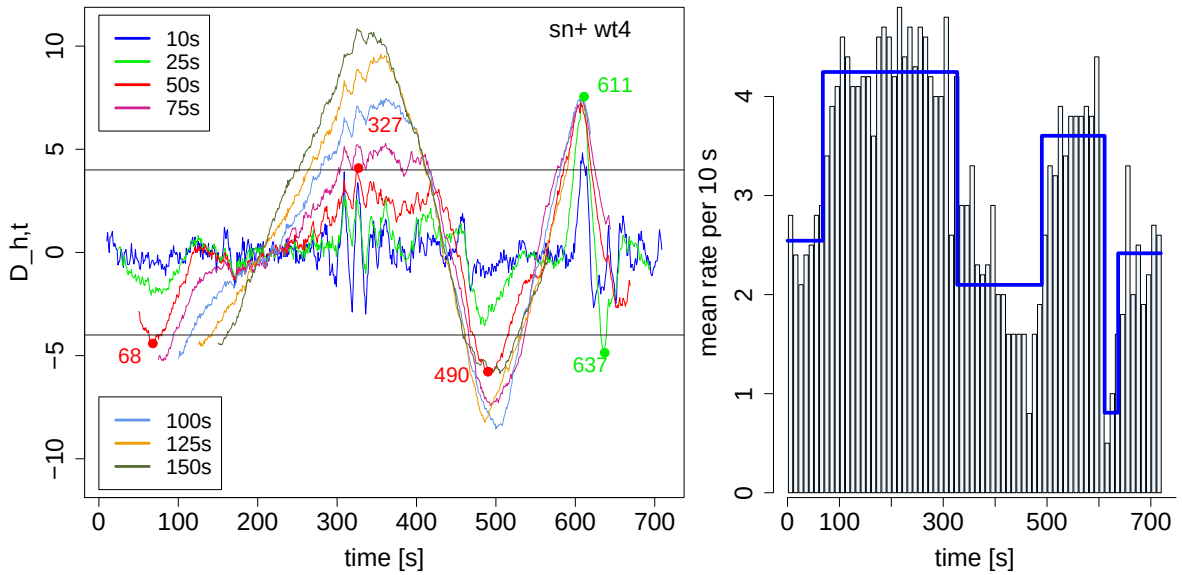

Figure 2.15: Application of the method to "sn+ wt4". The left picture shows the identified change points: 68s, 327s, 490s, 611s, 637s. The bar plot on the right presents the average intensity in intervals of length 10s. The blue line marks the estimated step rate function according to the located changes.

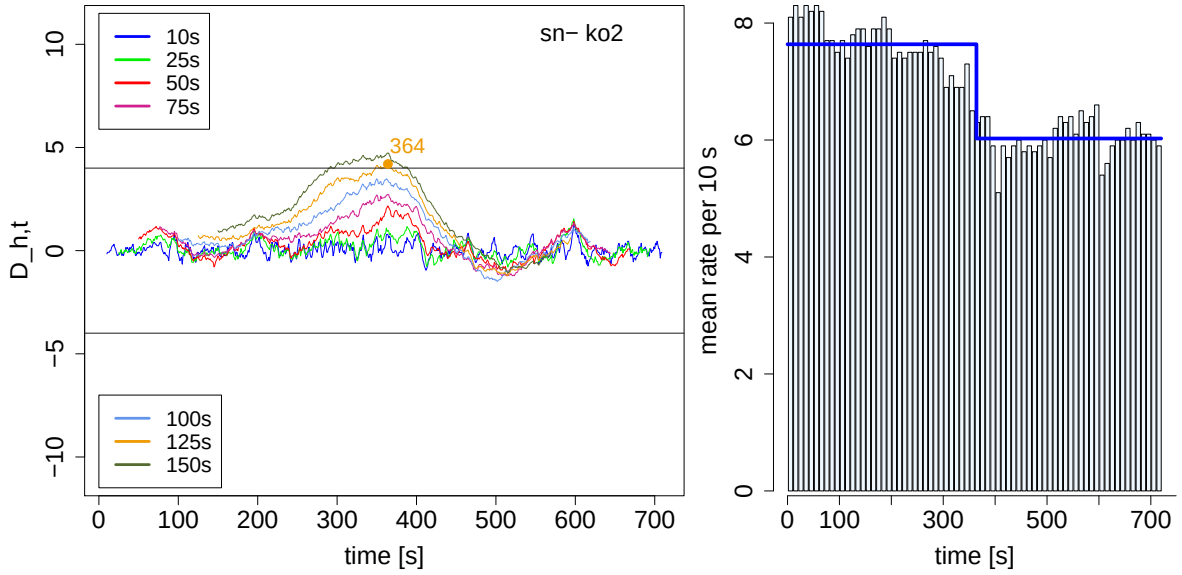

Figure 2.16: Application of the method to "sn- ko2". The left picture shows the identified change point: 364s. The bar plot on the right presents the average intensity in intervals of length 10s. The blue line marks the estimated step rate function according to the located change.

5. Spike train "sn- ko5"

Although there seems to be a short part around $t = 300s$ with lower intensity the Step-Filter-Test only detects a change at the end ($\hat{t}_{c_1} = 849s$) separating the spike train in a long lasting section with $\hat{\lambda}_1 = 4.85$ and a short lasting section with $\hat{\lambda}_2 = 2.2$ (see figure 2.17). This change was detected by $h = 50s$ as $h = 25s$ is obviously too small, but it can be suggested that $h = 30s$ or $h = 35s$ would have been pinpointed the change more accurately than $h = 50s$ because it seems that the length of the last section is less than 50s. In this case a finer adjustment of the smaller window sizes would have possibly performed better.

With regard to the break in the intensity in the first identified rate section, H_0 could not be rejected as the lines do not cross the boundary. This example illustrates that the assumption of an underlying Poisson process can limit the analysis as the spiking is sometimes more regular than in the poisson case. Hence, it is often more realistic to assume gamma distributed waiting times where the shape paramter κ allows for the adjustment of regularity of the corresponding spike train (see chapter 1).

In the case of "sn- ko5", if one describes the interval statistic by a gamma distribution, it is $\kappa > 1$ indicating a more regular occurence of the events. As a consequence, the range for which H_0 is not rejected would be smaller, which means $K < 4$, so that rate changes could have been detected more easily.

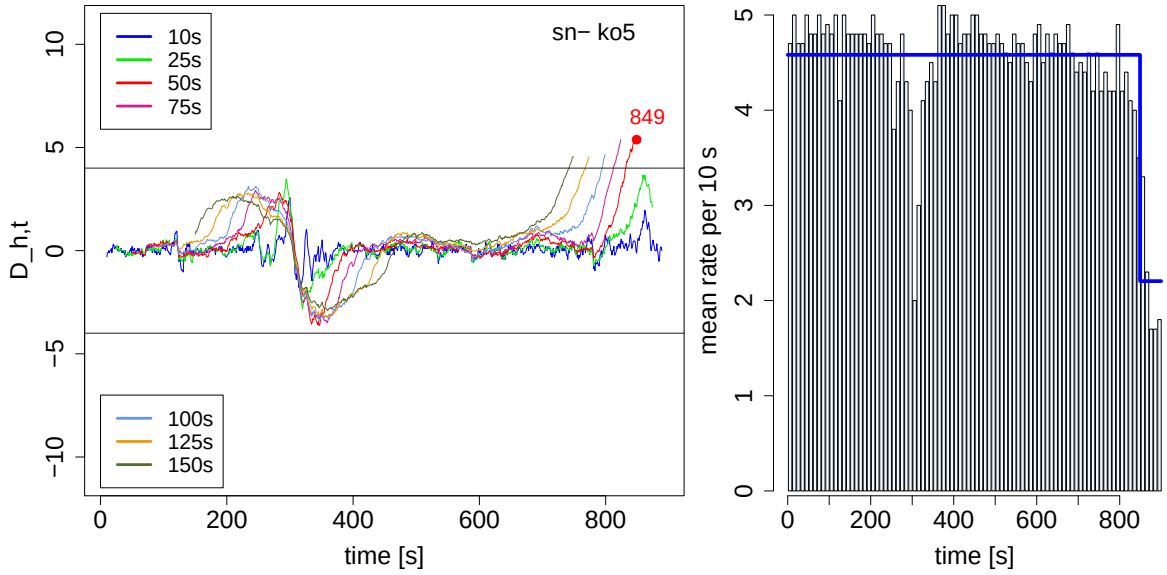

Figure 2.17: Application of the method to "sn- ko5". The left picture shows the identified change point: 849s. The bar plot on the right presents the average intensity in intervals of length 10s. The blue line marks the estimated step rate function according to the located change.

6. Spike train "sn- wt4"

In this example, figure 2.18, the test identifies four changes in the intensity yielding a separation of the spike train in five sections with estimated rates $\hat{\lambda}_1 = 6.12$, $\hat{\lambda}_2 = 4.22$, $\hat{\lambda}_3 = 6.18$, $\hat{\lambda}_4 = 4.1$ and $\hat{\lambda}_5 = 6.61$. The first rate change, $\hat{t}_{c_1} = 41s$, could just be detected by $h = 25s$. The other window sizes are too large for finding the change as the first section has an estimated duration of $41s$.

The fourth section consists of a short time where the intensity is lower, but this difference does not get significant i.e. H_0 is not rejected. Here, one can observe an increasing intensity from $476s$ to the end of the recording with approximately three steps where the first one is not identified as the difference between the first two steps is too small and the length of the sections short. This might be an example for an increase in the intensity which the method cannot identify.

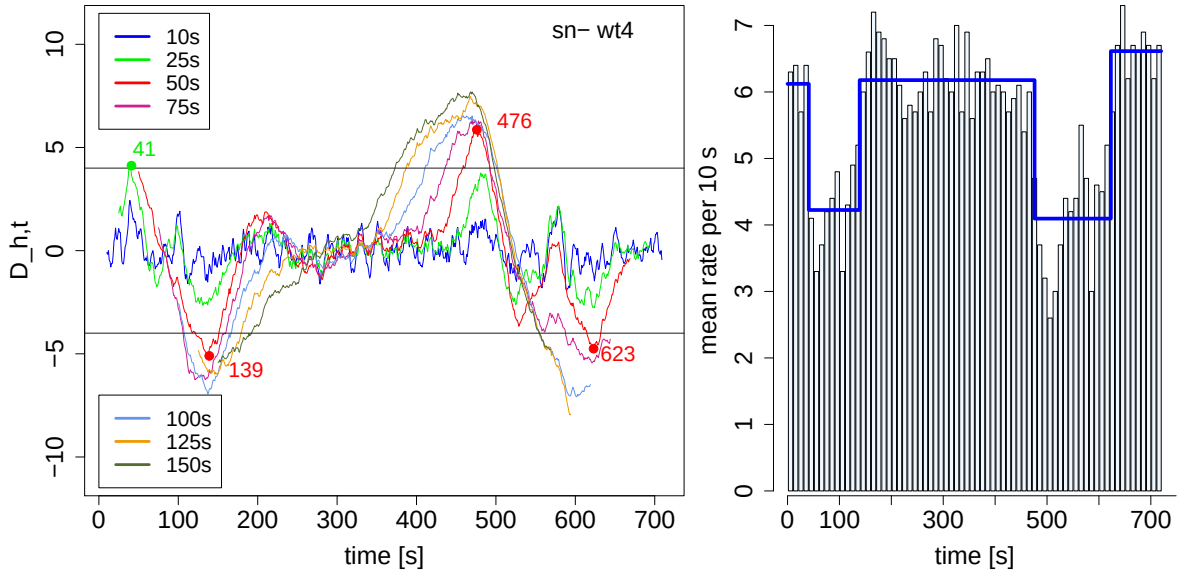

Figure 2.18: Application of the method to "sn- wt4". The left picture shows the identified change points: 41s, 139s, 476s, 623s. The bar plot on the right presents the average intensity in intervals of length 10s. The blue line marks the estimated step rate function according to the located changes.

2.3 Conclusion of chapter 2

The goal was to detect rate changes in firing intensity of spike trains under the assumption that the underlying probability distribution governing the number of spikes in intervals of length h is poisson. The presented method is based on the difference between normed spike counts in the adjacent time intervals $[t-h,t]$ and $(t,t+h]$ for different window sizes h and $t \in [h, T-h]$.

The main quantities influencing the performance of the test are the length of the rate sections, the hight of the rates in the two respective intervals and the difference between them. Generally, the test power is smaller if the rate sections are short as only small window sizes can locate the change. In addition, for a fixed window size h a small relative difference (the difference in relation to the hight of the rates) causes a lower test power. The reason is that very small differences in the intensity like $|\lambda_1 - \lambda_2| < 1$ are expected by chance in a Poisson process so they have a low probability to be detected. As the variance of spike counts is the greater the higher the rate parameter of the Poisson process, it is obviously that for the same $|\lambda_1 - \lambda_2|$ the difference between higher rates has a lower probability to be detected. But the probability grows when the rate sections are longer as larger window sizes can locate them. With respect to the quality of the estimate of the change point it can be concluded that the test performs

slightly better when the relative difference is large as the confidence interval for the point in time of the change is smaller.
The practicability of the method has been tested in simulations and by applying the method to real data. It can be concluded that the test is suitable for the detection of rate changes in spike trains provided that the intensity can be well approximated by a step rate function. The result suggests that for steps like $|\lambda_1 - \lambda_2| < 1$ the test power is in most cases too small. This means that an increase (decrease) in the intensity can hardly be identified as the approximated steps will be small.

3 Graphical approaches for the detection of rate changes

This chapter presents different ways to detect changes in the intensity of spike trains with underlying nonstationary Poisson process. They have been developed while working on a practical method which allows to locate changes in the intensity. First of all the approaches will be described and applied to simulations in order to demonstrate their capabilities through a number of examples. Afterwords they are one by one applied to the data so that their practicability can be compared.

3.1 Variability of spike counts

Consider a spike train generated by a stationary Poisson process with constant rate parameter λ. Dividing the spike train of T seconds in n disjount intervals of h seconds the expected number of spikes in each interval is λh. Because of the properties of a Poisson process the variance of the number of spikes is also λh and, divided by h, it is $\lambda \; \forall \; h$. Therefore, it is expected that for an arbitrary division of the spike train when counting the number of spikes in all intervals the variance of spike counts divided by h is λ. In the following the interest lies on the variability of spike counts in spike trains representing realizations of nonstationary Poisson processes. It will be expected that for those interval lengths h which divide the spike train into its different rate sections the variance of spike counts is maximal.

3.1.1 Estimation of the variance of spike counts

Imagine a spike train modeled by a nonstationary Poisson process with step rate function $r(t)$. The observed interspike intervals (ISIs) $\mathbf{Y}_i$ are exponential distributed with

$\mathbf{Y}_i \sim \text{Exp}(\lambda_1)$ in the first half and $\mathbf{Y}_i \sim \text{Exp}(\lambda_2)$ in the second half of the spike train. So $r(t)$ can be written as:

$$r(t) = \begin{cases} \lambda - a & \text{for t} \in \left[0, \frac{1}{2}T\right]; \lambda, a \in \mathbb{R} \\ \lambda + a & \text{for t} \in \left(\frac{1}{2}T, T\right]; \lambda, a \in \mathbb{R} \end{cases}$$

For the computation of the variability of spike counts the spike train is divided into $2n$ disjoint intervals ($n \in \mathbb{N}$) each of which has length h with $T = 2n \cdot h$ (see figure 3.1). The spikes in the ith observation window are poisson distributed according to a random variable $\mathbf{N}_i$, $i = 1, \ldots, 2n$ whereby
$\mathbf{N}_1, \ldots, \mathbf{N}_n$ are independent and Pois$((\lambda - a) \cdot h)$-distributed
$\mathbf{N}_{n+1} \ldots \mathbf{N}_{2n}$ are independent and Pois$((\lambda + a) \cdot h)$-distributed
In this process, it is ruled out that in an interval spikes occur with a rate composed of λ_1 and λ_2.

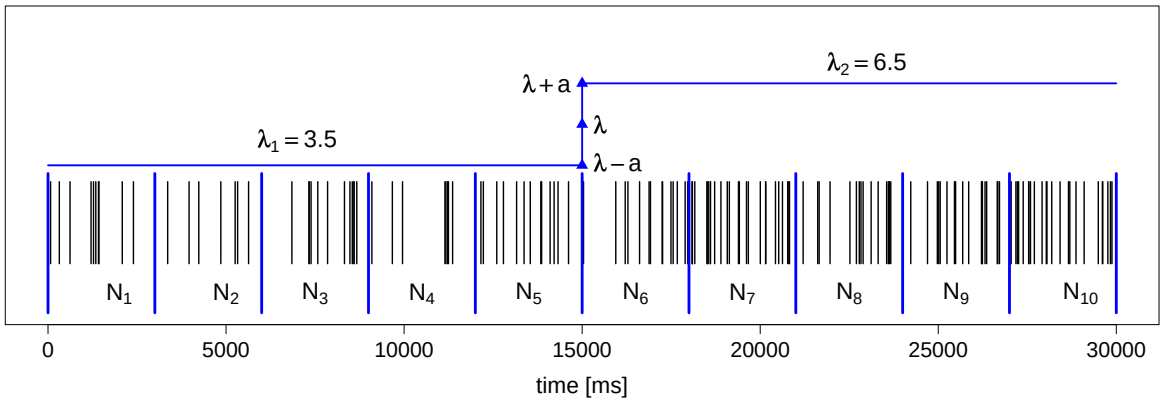

Figure 3.1: Simulated spike train with T=30s which is divided into 10 intervals of 3 seconds (n=5). The ISIs in first half of the spike train are Exp(λ_1)- and in the second half Exp(λ_2)-distributed.

Now the expected empirical variance of spike counts, which depends on n and h and will be denoted by $V_{h,n}$, is computed.

$$V_{h,n} = E\left[\frac{1}{(2n-1)}\sum_{i=1}^{2n}\left(\mathbf{N}_i - \bar{\mathbf{N}}\right)^2\right] = \frac{1}{(2n-1)}\sum_{i=1}^{2n} E\left[\left(\mathbf{N}_i - \bar{\mathbf{N}}\right)^2\right] \tag{3.1}$$

In order to simplify this calculation the summands are looked at separately whereby two cases can be distinguished:

1. i=1 $\Rightarrow \mathbf{N}_1$ is representative for $\mathbf{N}_2, \ldots, \mathbf{N}_n$ because they are i.i.d
2. i=2n $\Rightarrow \mathbf{N}_{2n}$ is representative for $\mathbf{N}_{n+1} \cdots \mathbf{N}_{2n-1}$ because they are i.i.d

First case: i=1

$$\begin{aligned} E\left[\left(\mathbf{N}_1-\bar{\mathbf{N}}\right)^2\right] &= E\left[\left(\left(1-\frac{1}{2n}\right)\mathbf{N}_1-\frac{1}{2n}\sum_{i=2}^{2n}\mathbf{N}_i\right)^2\right] \\ &= \underbrace{\mathrm{Var}\left[\left(1-\frac{1}{2n}\right)\mathbf{N}_1-\frac{1}{2n}\sum_{i=2}^{2n}\mathbf{N}_i\right]}_{\text{part }(a)}+\underbrace{\left(E\left[\left(1-\frac{1}{2n}\right)\mathbf{N}_1-\frac{1}{2n}\sum_{i=2}^{2n}\mathbf{N}_i\right]\right)^2}_{\text{part }(b)} \end{aligned}$$

For a better overwiev the two parts (a) and (b) are looked at separately.

$$\begin{aligned} (a)\quad & \left(\frac{2n-1}{2n}\right)^2\mathrm{Var}\left[\mathbf{N}_1\right]+\frac{1}{4n^2}\left[(n-1)\,\mathrm{Var}\left[\mathbf{N}_1\right]+n\mathrm{Var}\left[\mathbf{N}_{2n}\right]\right] \\ = \quad & \frac{(2n-1)^2}{4n^2}(\lambda-a)\,h+\frac{(n-1)}{4n^2}(\lambda-a)\,h+\frac{n}{4n^2}(\lambda+a)\,h \\ = \quad & \frac{1}{4n^2}\left[(2n-1)^2(\lambda-a)\,h+(n-1)(\lambda-a)\,h+n(\lambda+a)\,h\right] \\ = \quad & \frac{1}{4n^2}\left[\left(4n^2-2n\right)\lambda h-\left(4n^2-4n\right)ah\right] \\ = \quad & \frac{(2n-1)}{2n}\lambda h-\frac{(n-1)}{n}ah \end{aligned}$$

$$\begin{aligned} (b)\quad & \left[\left(\frac{2n-1}{n}\right)E\left[\mathbf{N}_1\right]-\frac{1}{2n}\left((n-1)\,E\left[\mathbf{N}_1\right]+nE\left[\mathbf{N}_{2n}\right]\right)\right]^2 \\ = \quad & \left[\frac{2n-1}{n}(\lambda-a)\,h-\frac{1}{2n}\left[(n-1)(\lambda-a)+n(\lambda+a)\,h\right]\right]^2 \\ = \quad & \frac{1}{4n^2}\left[(2n-1)(\lambda-a)\,h-(n-1)(\lambda-a)\,h-n(\lambda+a)\,h\right]^2 \\ = \quad & \frac{1}{4n^2}\left(-2nah\right)^2=a^2h^2 \end{aligned}$$

Putting the results of (a) and (b) together equation 3.1 for i=1 is

$$E\left[\left(\mathbf{N}_1-\bar{\mathbf{N}}\right)^2\right]=\frac{(2n-1)}{2n}\lambda h-\frac{(n-1)}{n}ah+a^2h^2 \tag{3.2}$$

Second case: i=2n

The computation of the variability for i=2n is analogous to the first case and equation (3.2) transforms to

$$E\left[\left(\mathbf{N}_{2n}-\bar{\mathbf{N}}\right)^2\right]=\frac{(2n-1)}{2n}\lambda h+\frac{(n-1)}{n}ah+a^2h^2 \tag{3.3}$$

So the two cases differ from each other only with regard to the sign of the middle term and inserting the extensions into equation 3.1 yields

$$\begin{aligned} V_{h,n} &= \frac{1}{(2n-1)} \sum_{i=1}^{2n} E\left[\left(\mathbf{N}_i - \bar{\mathbf{N}}\right)^2\right] \\ &= \frac{1}{(2n-1)} \left(nE\left[\left(\mathbf{N}_1 - \bar{\mathbf{N}}\right)^2\right] + nE\left[\left(\mathbf{N}_{2n} - \bar{\mathbf{N}}\right)^2\right]\right) \\ &= \frac{n}{(2n-1)} \left(\frac{2(2n-1)}{2n}\lambda h + 2a^2h^2\right) \\ &= \lambda h + \frac{2n}{(2n-1)}a^2h^2 \end{aligned} \tag{3.4}$$

In order to get comparable results for the different divisions of the spike train equation 3.4 has to be divided by h:

$$\boxed{\frac{V_{h,n}}{h} = \lambda + \frac{2n}{(2n-1)}a^2h} \tag{3.5}$$

Note that at the beginning the spike train was divided into $2n$ intervals with $n = 1, 2, \ldots, \frac{T}{2}$. For a given n the length of the intervals h can be derived from $h = \frac{T}{2n}$. This means that equation 3.5 is only exact for those window sizes h which arise from a given n. In addition $2n$ can be replaced by $2n = \frac{T}{h}$ so that only one variable is left.

$$\boxed{\frac{V_h}{h} = \lambda + \frac{T}{(T-h)}a^2h} \tag{3.6}$$

Equation 3.6 shows that the empirical variance increases with growing h. It will take its maximum in $h = \frac{T}{2}$ which is the last possible window size for which the spike train can still be divided in two intervals.

3.1.2 Application to simulations

On the left in figure 3.2 the black triangles mark the theoretical values of the empirical variance of spike counts (see equation 3.5) for designated h as a function of the number of intervals. The parameter T, a and λ are taken from the underlying Poisson process of the simulated spike train where the results for the variance divided by h for $h \in \{1, 2, \ldots, 350\}$ are presented by the blue points in figure 3.2. Note that the division does not work out precisely when $n = \frac{T}{2h} \notin \mathbb{N}$. In this case the end of the spike train is truncated so that an exact division in $n \in \mathbb{N}$ intervals of h seconds is possible. Often the reduction of the whole length of the spike train causes that the variance falls strikingly because a long part of one rate section is cut away if the window size is large (see figure

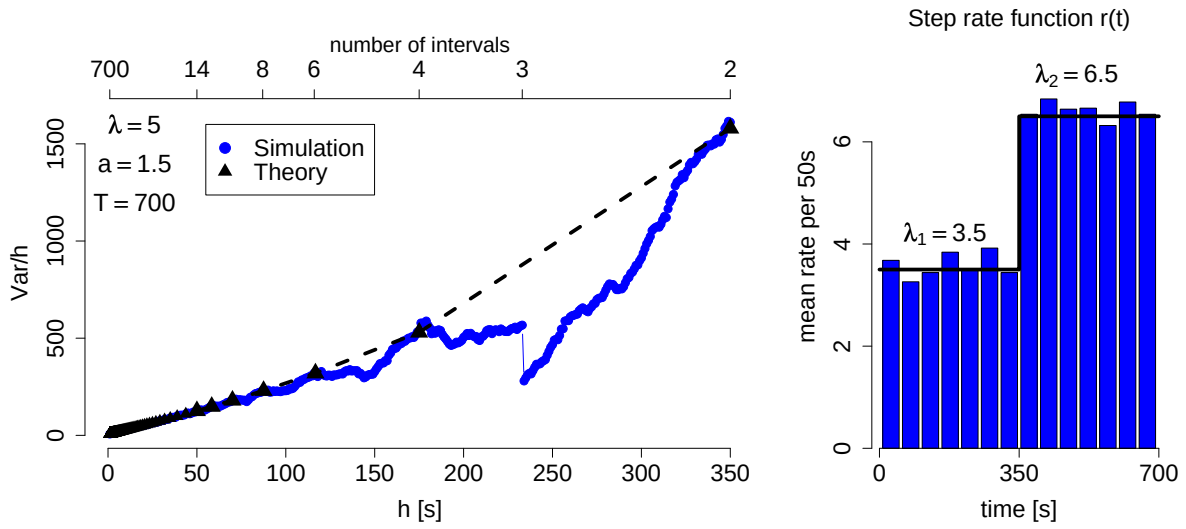

Figure 3.2: Variability of spike counts (filled blue circles) for different values of h of a simulated Poisson process with $T = 700s$, $a = 1.5$, $\lambda = 5$. The black triangles mark the estimated empirical variability $\frac{V_{h,n}}{h}$. On the right the estimated intensity in intervals of length 50s and the true rate function $r(t)$ are presented.

3.2: $n = 3 \rightarrow n = 2$ at time point $t = 234$). This phenomenon is also exemplified in figure 3.3: reducing the number of intervals by one, like $n = 4$ ($h = 163$) to $n = 3$ ($h = 164$), causes a decrease in the variance.

In summarising it can be stated that the variability increases until h comprises the whole rate section, namely $h = \frac{T}{2}$, which is the moment of the rate change. Note that for growing h, the number of intervals decreases so that finally the variance is computed over two intervals which means that the computation is not very stable.

When applying the method to simulated spike trains with underlying Poisson processes, it can be seen that the theoretical findings can only be extended to other step rate functions when all steps respectively all rate sections have the same length l or when the intensity changes only once. In those cases the variability increases for growing h until $h = l$ in accordance to the theoretical results which means that the window size for which the empirical variance is maximal, termed h_{max}, equals the time scale on which the rate changes (see figure 3.3). However, if the length of the rate sections differ from each other then h_{max} is not very meaningful. It gives only the information that for this window size the division in sections with equal length yields the maximal variability of spike counts but it is not possible to directly point to the course of the intensity.

To get further information one can apply the method again to those parts of the spike train which have been obtained after the separation according to h_{max}. However, it is still difficult to draw conclusions from the identified h_{max} in each part as the interpretation of the empirical variance-profile is ambiguous.

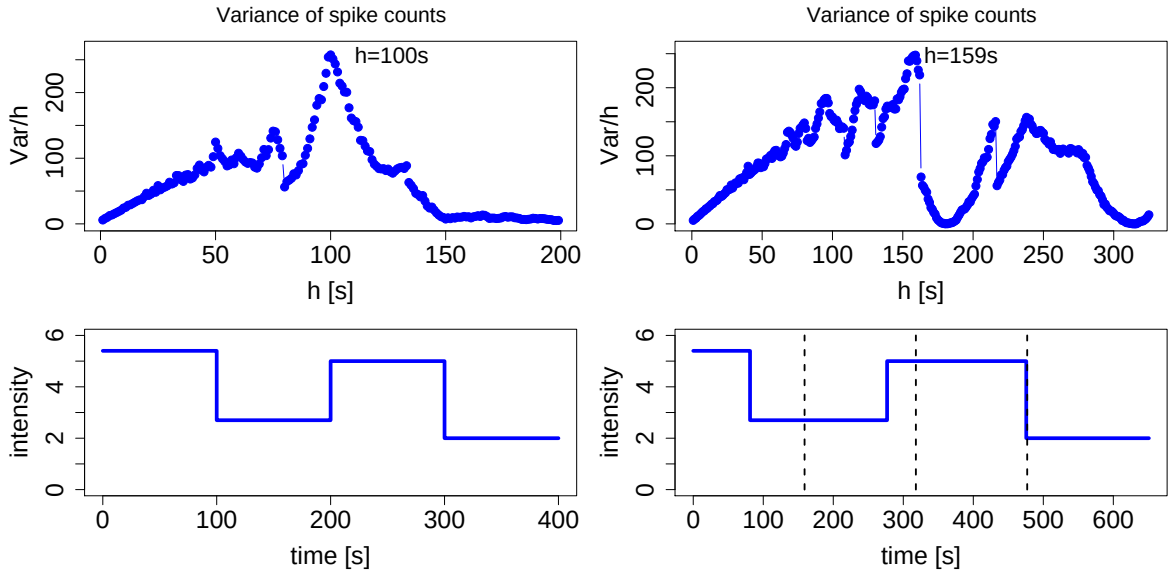

Figure 3.3: Variability of spike counts for two simulated spike trains modeled by Poisson processes with different intensities. Left: the four rate sections have all length $l = 100s$ which equals the window size for which the empirical variance is maximal; Right: the four rate sections differ in their length. Here, the window size which causes the maximal variance ($h = 159s$) is the one for which the spike train can just be divided in four parts (see dashed lines in the rate profile).

To sum up, the hope to identify different time scales on which the intensity of the underlying Poisson process changes based on the calculation of the empirical variance of spike counts has not been fullfilled. The greatest deficit of the method is the division of the spike train in nonoverlapping intervals, so that the interpretation of the results considering the rate changes has no theoretical foundation if the lengths of the individual sections differ. In addition, the number of intervals decreases very quickly for growing h so that the computation of the empirical variance is not stable from a certain window size. Moreover, the division of the spike train in disjoint intervals is often incomplete so that the empirical variance falls only as a consequence of not including the whole spike train into the calculation.

As a result, the next approach compares spike counts in overlapping intervals which makes it possible to visualize changes in the intensity of spiking although they happen on different time scales.

3.2 Comparison of normed spike counts in overlapping intervals

Consider now, that a spike train is divided into overlapping intervals of length $h[s]$. We count the number N of spikes in the intervals $[1, h+1]; [2, h+2]; \ldots; [T-h, T]$ so that one gets $N_i = N(i-1, h+i-1)$ for $i = 1, 2, \ldots, n_h$ with $n_h = (T-h)+1$. Afterwards the spike counts are standardised by the estimated intensity of the underlying Poisson process $\hat{\lambda} = \dfrac{\mathbf{N}(T)}{T}$ yielding

$$Z_i^h = \frac{N_i - \hat{\lambda}h}{\sqrt{\hat{\lambda}h}}$$

This can be done for different window sizes h with $h = 1, 2, \ldots, \frac{T}{2}$ so one gets all in all $n_1 \cdot n_2 \cdot \ldots \cdot n_{T/2}$ values for Z_i^h. Next, out of all these values 3000 are taken randomly and afterwords the corresponding h is plotted against Z_i^h (see figure 3.4). For the presentation of the points (h, Z_i^h) a colour-code is used which shall help to identify the position of the interval to which the selected Z_i^h belongs:

- red point $\Rightarrow$ the belonging interval $[a, b]$ is from the first part so $0 \leq a < \frac{T}{2} - h$ and $h \leq b < \frac{T}{2}$
- green point $\Rightarrow$ the belonging interval $[a, b]$ is from the middle part so $\frac{T}{2} - h \leq a \leq \frac{T}{2}$ and $\frac{T}{2} \leq b < \frac{T}{2} + h$
- blue point $\Rightarrow$ the belonging interval $[a, b]$ is from the posterior part so $\frac{T}{2} < a < T - h$ and $\frac{T}{2} + h < b \leq T$

Figure 3.4 exemplifies the realization of the procedure described above by means of two simulated Poisson processes with different intensities.
In the first case, a Poisson process with constant firing rate, the points fluctuate around zero with $E[Z_i^h] = 0$ and $\mathrm{Var}[Z_i^h] = 1$ according to the standardisation. But it can be seen, that for smaller window sizes the variation of the points is greater which can be attributed to averaging over smaller time intervals and having more nonoverlapping windows i.e more independent Z_i^h.
In the second case the intensity of the Poisson process changes at time $\frac{T}{2}$ whereby in the first half of the time the intensity is smaller than in the second half, i.e. $\lambda_1 < \hat{\lambda} < \lambda_2$. This can be seen in the figure as only the red points lie under and only the blue points above the zero baseline. The green points belong to intervals which contain the time point of the rate change so both rates are included each time with different shares. In addition the blue respectively red points fluctuate around an imaginary line which can

be described as a root function given by $f_i(h) = c_i \cdot \sqrt{h}$ according to the expectation of Z_i^h

$$E[Z_i^h] = \frac{E[N_i] - \hat{\lambda}h}{\sqrt{\hat{\lambda}h}} = \frac{\lambda_i - \hat{\lambda}}{\sqrt{\hat{\lambda}}} \cdot \sqrt{h}$$

so the parameter c_i can be identified as

$$c_1 = \frac{\lambda_1 - \hat{\lambda}}{\sqrt{\hat{\lambda}}} \text{ and } c_2 = \frac{\lambda_2 - \hat{\lambda}}{\sqrt{\hat{\lambda}}}$$

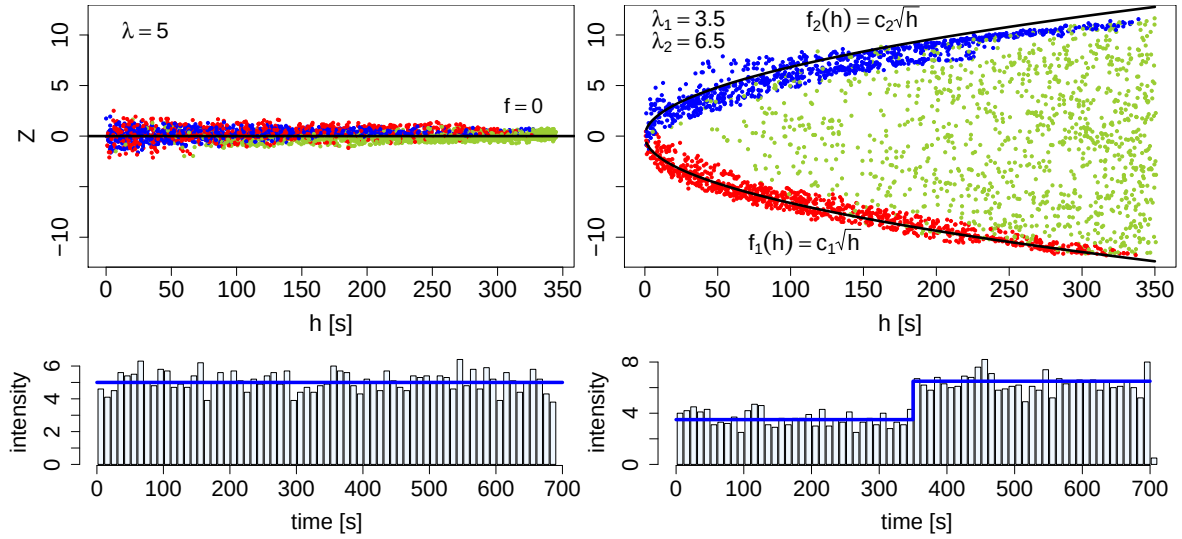

Figure 3.4: Left: Normed spike counts of a Poisson process with intensity $\lambda(t) \equiv 5$ and $f(h) = E[Z_i^h] \equiv 0$. Right: Normed spike counts of a Poisson process where the rate changes at time $\frac{T}{2}$ with characteristic root function $f_i(h) = c_i \cdot \sqrt{h}$ (see text).

Having more then one rate change the red, blue and green points will intermingle and one can see characteristic structures which allow to make an educated guess concerning the intensity of the underlying Poisson process in comparison to $\hat{\lambda}$ in the first, middle and posterior part of the spike train. For example in figure 3.5 one can conclude that the intensity is smaller than $\hat{\lambda}$ for a long time in the first part as red points are going down approximately from 0 for $h = 1s$ to -10.5 for $h = 180s$. But there seems to be an interval with intensity bigger than $\hat{\lambda}$ as well because some of the red points are also above the zero baseline. In the middle of the spike train the intensity seems to be bigger than $\hat{\lambda}$ and the posterior part includes intensities smaller as well as bigger than $\hat{\lambda}$ as blue points are above and below the zero line whereas this is only true for smaller window sizes. For higher values of h the blue points are only above the zero line so one can conclude that the rate section of the lower intensity is not so long.

It has been learned that one has to search for characteristic lines in the cluster of points as it has already been indicated before when identifying the square root functions in

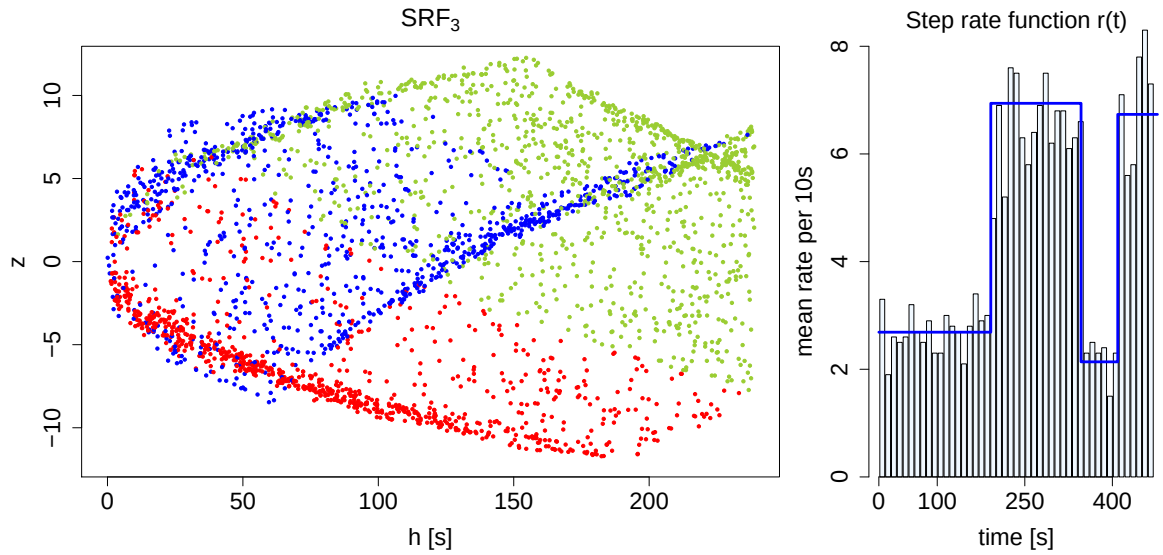

Figure 3.5: Presentation of the normed number of spikes as points of a simulated spike train with three changes in the intensity (SRF_3). The firing rate is illustrated on the right.

figure 3.4. For example, in figure 3.5 the red points going down approximately from 0 for $h = 1s$ to -10.5 for $h = 180s$ can be connected by a line indicating that there is a rate section with intensity smaller than $\hat{\lambda}$ lasting about 180s.
This idea will be persued in the following where the presentation of the normed spike counts as points is replaced by characteristic lines which provide further information and finally improve the visualization of the course of the intensity.

3.3 Visualization of the course of the intensity

Let k be chosen randomly out of $[2, T-2]$ and taken as the centre of a series of intervals with growing length in the following way

1. $k \in [0, \frac{T}{2}] \Rightarrow [k-1, k+1]; [k-2, k+2]; \ldots; [0, 2k]$
2. $k \in [\frac{T}{2}, T] \Rightarrow [k-1, k+1]; [k-2, k+2]; \ldots; [T-2k, T]$

For every interval the number of spikes is determined and normed in the way described before. After that, the length of the corresponding intervals is plotted against the normed spike counts and one will get a line describing the progress of the intensity originating from k. This means that as long as $[k-i, k+i]$, $i \in \{1, 2 \ldots, n_k\}$ with n_k depending on the position of k in the spike train (see cases above), contains no rate change the line is approximately a square root function $f(h) = c \cdot \sqrt{h}$ with $c = \dfrac{\lambda_j - \hat{\lambda}}{\sqrt{\hat{\lambda}}}$

where λ_j is the intensity of the relevant rate section. But if $[k-(i+1), k+(i+1)]$ for some i between 1 and n_k covers a rate change then there will be a break in the characteristic root function at time $h = 2 \cdot i$. So if one identifies the break-point $h_b = 2i$ one can compute an estimation of the moment of the rate change:

$$\hat{t}_c = \begin{cases} k + 0.5 \cdot h_b & \text{for} \quad t_c > k \\ k - 0.5 \cdot h_b & \text{for} \quad t_c < k \end{cases}$$

As an example, figure 3.6 shows the characteristic lines for $4 \cdot 5$ randomly selected k out of the four parts of the spike train (see colour-code below).

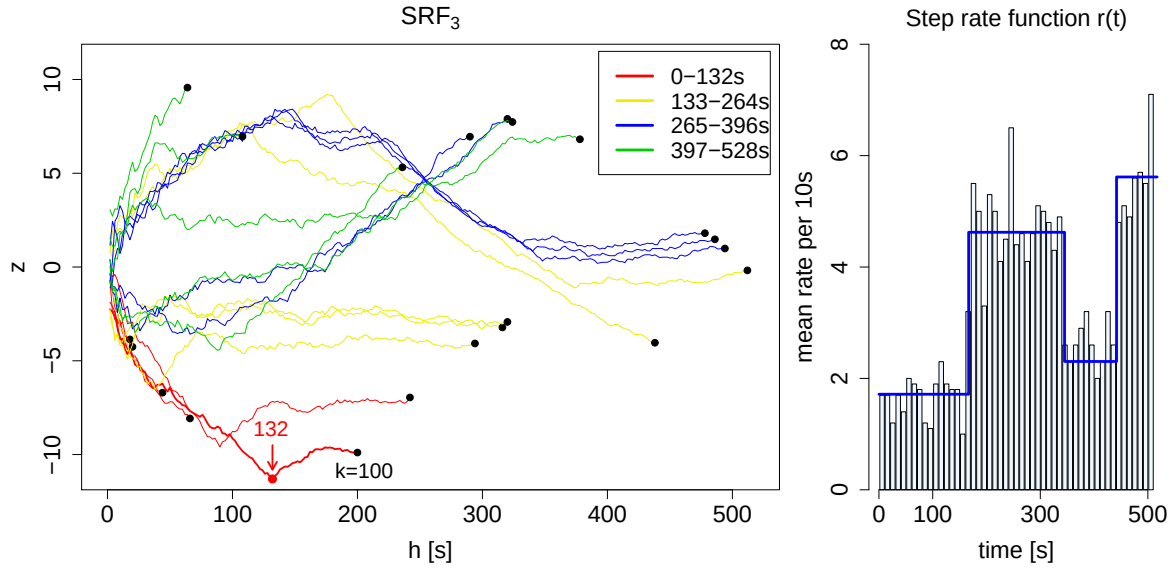

Figure 3.6: Presentation of the normed number of spikes as lines (see text). The x-axis indicates the length of the interval.

The length of a line corresponds to the position of k: for k in the front or posterior part the lines are shorter because of getting sooner to 0 or T when expanding the interval. In addition a colour-code is used again in order to be able to assign k to a specified time window:

- red lines $\Rightarrow k \in [0, \frac{T}{4}]$
- yellow lines $\Rightarrow k \in (\frac{T}{4}, \frac{T}{2}]$
- blue lines $\Rightarrow k \in (\frac{T}{2}, \frac{3T}{4}]$
- green lines $\Rightarrow k \in (\frac{3T}{4}, T]$

In order to describe the intensity of the underlying Poisson process of the spike train presented in figure 3.6 by means of the lines, one has to start at the beginning i.e. with

the red lines. It can be seen that at the beginning the intensity is smaller than $\hat{\lambda}$ as the red lines are below zero. For determining the first moment where the intensity changes one has to look for the break-points. For example, taking the red line which belongs to $k = 100$ it is $h_b = 132$ and therefore one can assume that $\hat{t}_{c_1} = 100 + 0.5 \cdot 132 = 166$. As long as $k < t_{c_1}$ the yellow lines are also below zero but for $k > t_{c_1}$ they are above zero as the intensity in the second rate section is bigger than $\hat{\lambda}$. Again the break-points can be identified. As the second rate section is sourrounded by two others one has to consider that depending on the position of k the intensity in $[k - i, k + i]$ can be influenced from both sides (see figure 3.7):

1. $\hat{t}_{c_1} = k - 0.5 \cdot h_b$ for $|k - t_{c_1}| < |k - t_{c_2}|$
2. $\hat{t}_{c_2} = k + 0.5 \cdot h_b$ for $|k - t_{c_1}| > |k - t_{c_2}|$

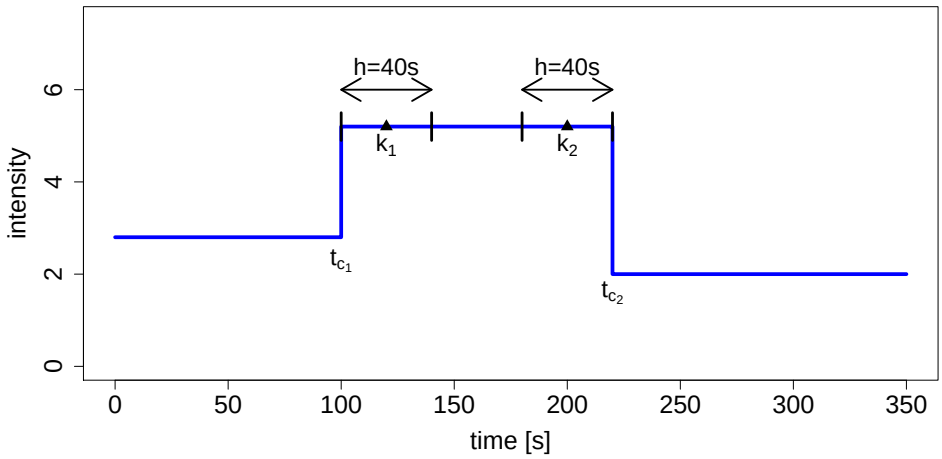

Figure 3.7: For $k_1 = 120s$ the identification of $h_b = 40s$ would lead to $\hat{t}_{c_1}$ and for $k_2 = 180s$ to $\hat{t}_{c_2}$.

To conclude, it is much effort to approximate the course of the firing rate with the described graphical technique. In order to resolve this problem, the interval $[k, k + 1]$ $(h = 1s)$ with origin k is only expanded in the right direction so that the break-points can immediately be assigned to changes in the intensity of spiking.

3.4 Identification of the break-points as potential change points

After having chosen a random k out of $[0, T-1]$ the following series of intervals are considered:

$$[k, k+1]; [k, k+2]; \ldots; [k+k+h]; \ldots; [k, T]$$

with window sizes $h = 1, \ldots, T$. In every one of those intervals the spikes are counted and afterwards the numbers are normed as described above. When presenting the resulting Z_h^k the allocated value on the x-axis will be the end point $k+h$ of the particular interval (see figure 3.8). As long as $[k, k+h]$, $i = 1, 2, \ldots, T$, contains no rate change the values for Z_h^k will approximately describe a square root function $f(h) = c \cdot \sqrt{h}$ with $c = \frac{\lambda_j - \hat{\lambda}}{\sqrt{\hat{\lambda}}}$ where λ_i is the intensity of the relevant rate section. Once $[k, k+h]$ contains two different intensities there will be a break in the line as the Z_h^k will no longer vary around the expected root function. The break-point can immediately be taken as an estimator for the moment of the rate change.
Figure 3.8 shows the application of the method to the simulated Poisson process from above (figure 3.6) whereby 30 values for k have been selected randomly out of $[0, T-1]$.

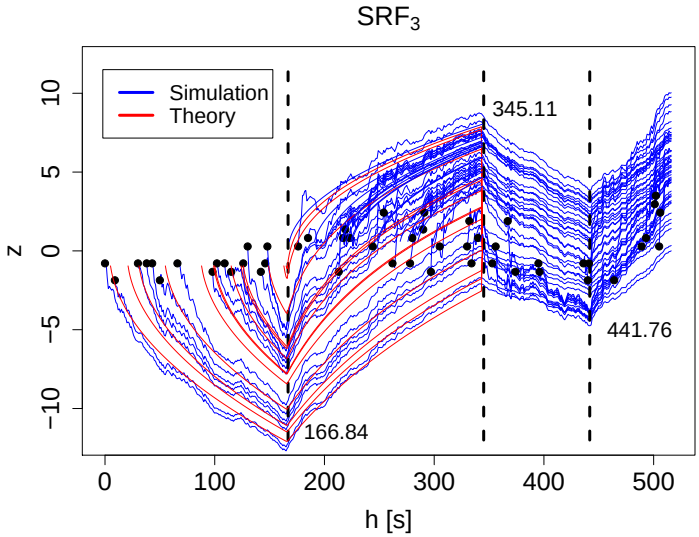

Figure 3.8: Presentation of the normed number of spikes (blue lines) of a spike train modeled by a Poisson process with three changes in the intensity (SRF_3). The dashed lines mark the true change points of the intensity ($t_{c_1} = 166.84$, $t_{c_2} = 345.11$, $t_{c_3} = 441.76$) which correspond to the particular break-points. The red lines are those which one can expect for the first rate change.

The true point in times of the rate changes are marked by the dashed lines and one

can see that the break-points of the lines match. In addition, the red lines show for the first rate change $t_{c_1} = 166.84$ the course of the Z_h^k in expectation. Hence

$$E[Z_h^k] = \begin{cases} \dfrac{\lambda_1 - \hat{\lambda}}{\sqrt{\hat{\lambda}}}\sqrt{h} & \text{for} \quad h \leq (t_{c_1} - k) \\ \dfrac{(\lambda_1 - \lambda_2)(t_{c_1} - k)}{\sqrt{\hat{\lambda} h}} + \dfrac{\lambda_2 - \hat{\lambda}}{\sqrt{\hat{\lambda}}}\sqrt{h} & \text{for} \quad h > (t_{c_1} - k) \end{cases}$$

with h = window width, λ_i = intensity of the ith rate section and $\hat{\lambda}$ = average intensity of the whole process.

For every $k \in \{0, 1, 2, \ldots (T-1)\}$ (for every line) the break-point can be identified. Therefore, the minimum respectively maximum depending on whether the line starts below or above zero is determined (see figure 3.9). Here $Z_5^k = \dfrac{N(k, k+5) - \hat{\lambda}}{\hat{\lambda}}$ is taken as the indicator for the decision whether to take the minumum or maximum in order to avoid false decisions caused by random variations like $Z_1^k > 0$ although the intensity of the rate section is smaller $\hat{\lambda}$. Having identified all break-points it seems to be reasonable to take only the accumulation points as estimators for t_{c_i} (see figure 3.9).

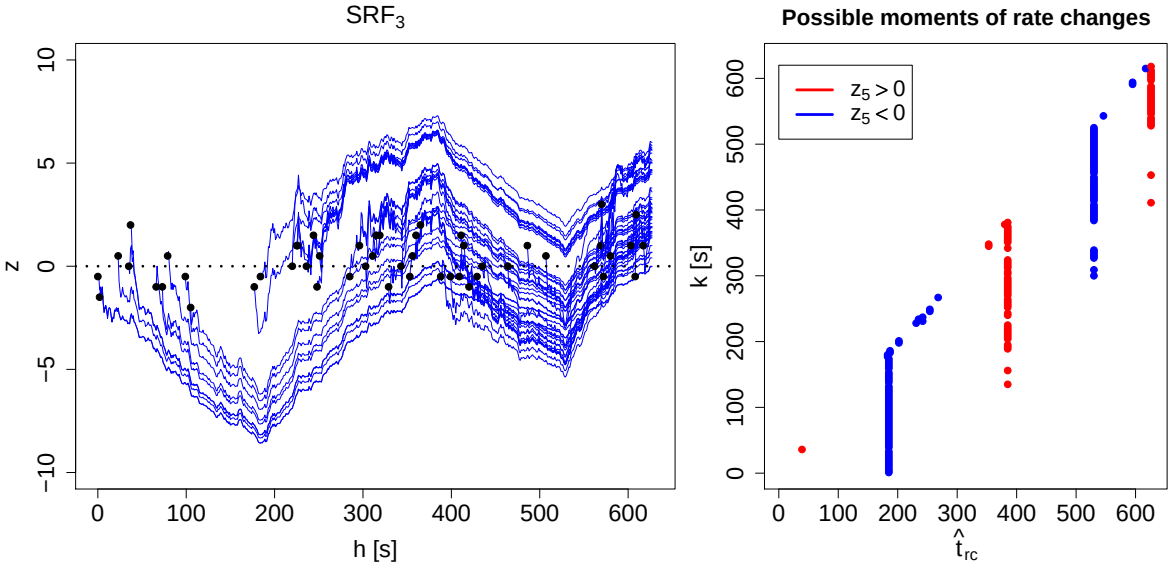

Figure 3.9: Left: Normed number of spikes of a spike train modeled by a Poisson process with three changes in the intensity (SRF_3). Right: Identified break-point of every line (starting point k) with red point $\hat{=}$ $Z_5 > 0$ and blue point $\hat{=}$ $Z_5 < 0$.

However, problems occur if the minima or maxima cannot clearly be identified like having a rate section where the intensity is nearly $\hat{\lambda}$ or having peaks which dominate so that others are not considered. In addition, having a homogeneous Poisson process one can also identify break-points which sometimes cumulate in one point in time so that a rate change could erroneously be assumed.

In order to decide for every identified break-point wheather or not to reject stationarity of the firing rate (null model) a decision rule has to be developed. In an attempt to establish a statistical test the Step-Filter-Method (see chapter 2) was developed.

3.5 Application to real data

The spike train "sn- wt8" is chosen in order to exemplify the practical use of the described methods.

3.5.1 Empirical variance of spike counts

Figure 3.10 shows the determination of the length of the interval h for which the empirical variance of the number of spikes is maximal (h_{max}). Taking this window size, namely $h_{max} = 87s$, as time scale on which the firing rate changes one can divide the spike train into sections of length $87s$ and compute the intensity in there. The resulting rate function can be seen in figure 3.10 in form of the blue line.

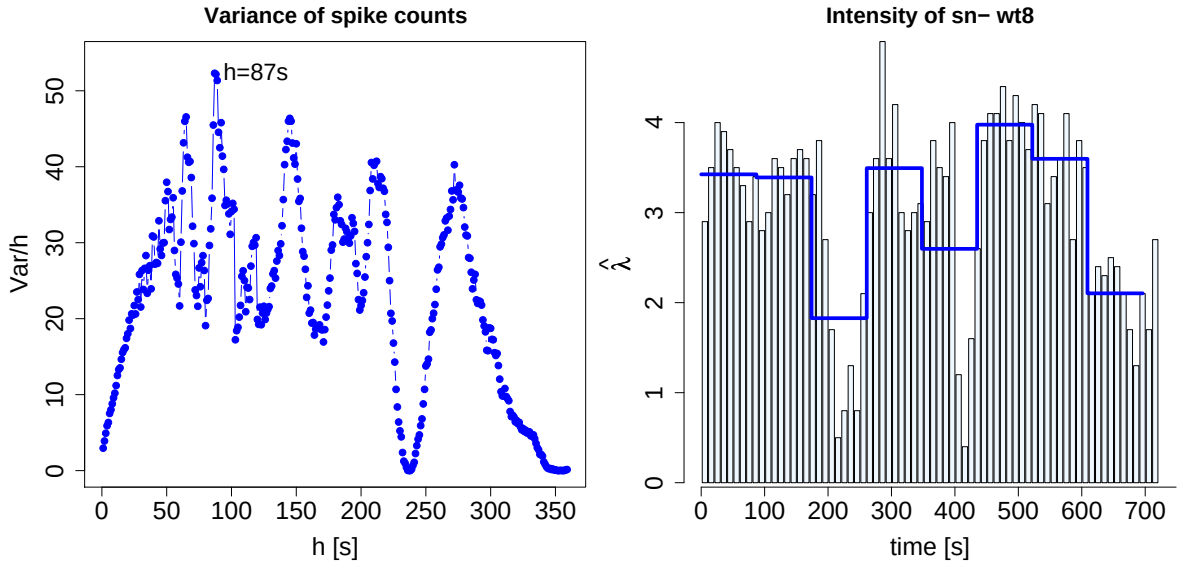

Figure 3.10: Left: Empirical variance of spike counts for different window sizes h. Right: Rate profile of "sn- wt8". The blue line marks the average intensity in intervals of length $h_{max} = 87s \mathrel{\hat{=}}$ window size for which the empirical variance is maximal.

Obviously, this rate profile does not fit very well to the true course of the intensity (see for example the intensity of "sn- wt8" around the time point $t = 400s$) so it can be concluded that the division in sections of equal length is not appropriate.

3.5.2 Visualization of the course of the intensity

The presentation of the normed spike counts determined out of overlapping intervals makes it possible to describe the progress of the intensity in comparison to the estimated intensity of the whole spike train $\hat{\lambda} = \frac{N(T)}{T}$.
In the cluster of points one can see that in the first part (red points) seems to be rate sections of intensity bigger as well as smaller $\hat{\lambda}$. Near $(T/2)$ (green points, small h) the intensity is bigger than the $\hat{\lambda}$ and in the posterior part (blue points) one can again assume intensities smaller and bigger than $\hat{\lambda}$.

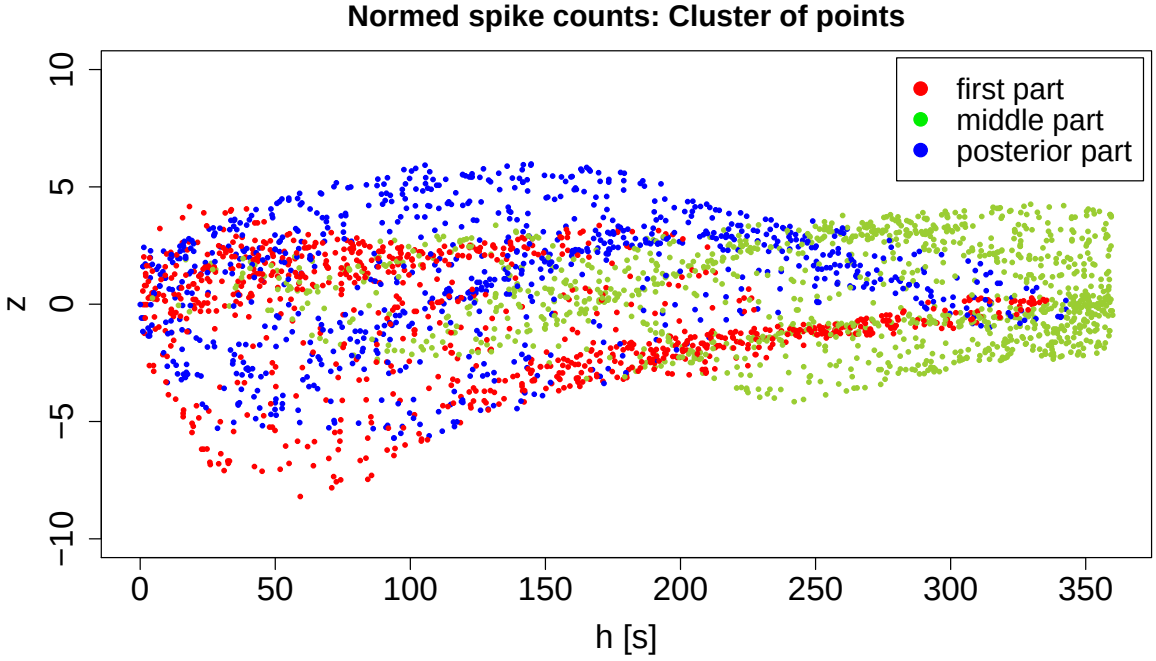

Figure 3.11: Presentation of a random sample of normed spike counts as points where the x-axis indicates the length of the interval.

However, the points alone do not visualize the whole course of the intensity. The extra information in terms of the characteristic lines originating from different time points k is necessary. They show in which way the normed spike numbers change when expanding the interval around k.
For the dataset "sn- ko8" one finds that the intensity right at the beginning is bigger than $\hat{\lambda}$ for about 180s as all red lines start above zero. It follows a section with lower spiking (the red lines go down and the yellow lines start below zero). This one seems to be shorter because there are yellow lines (those where k is near $T/2$) which start above zero as well indicating a section with intensity bigger than $\hat{\lambda}$. After that there is again a short section with lower intensity (the long blue lines start below zero) whereon one

with higher intensity follows which lasts longer (blue lines and green lines start above zero). As there is also a green line below zero it seems that in the end the intensity goes down again.

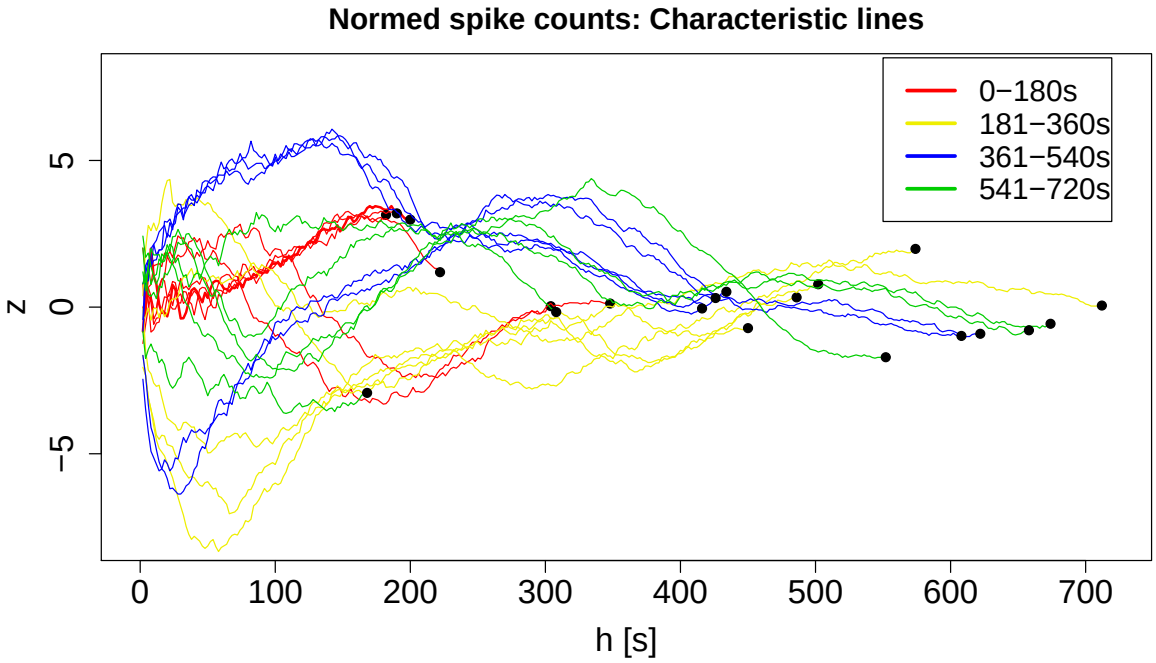

Figure 3.12: Characteristic lines originating from different time points k. The x-axis indicates the length of the interval.

Having a description of a possible course of the intensity the goal is now to determine concrete change points of the intensity.

3.5.3 Identification of break-points as potential change points

Figure 3.13 shows the identified break-points for 400 randomly selected $k \in [1, T-5]$. It seems that the one between 261s and 436s could not have been detected because the three break-points afterwards (the red ones) dominate so that all lines with $k > 216s$ starting above zero have their maximum at 544s, 583s or 611s. Here it is not clear which break-point is the true point in time where the intensity changes. For the estimation of the intensity (see image down right) the last one (611s) was taken as it is the one where the most points accumulate.

However, one cannot make significant statements about the estimated change points as it is not clear whether the break-points have to be taken seriously or not. In an attempt to adress this problem the Step-Filter-Method is applied to the spike train

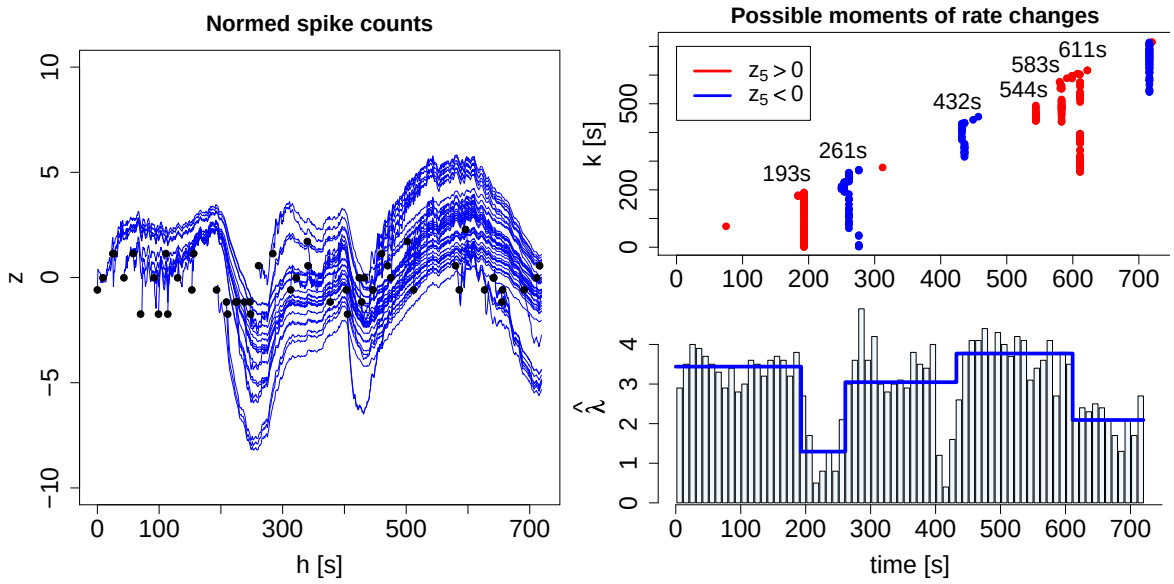

Figure 3.13: Left: Normed spike counts in intervals originating from k. Top right: Identified break-points which can be taken as potential change points. Down right: rate profile with estimated rate function out of the identified break-points (blue line).

"sn- wt8".

Step-Filter-Test

The test detects five rate changes: $\hat{t}_{c_1} = 207$, $\hat{t}_{c_2} = 263$, $\hat{t}_{c_3} = 406$, $\hat{t}_{c_4} = 431$, $\hat{t}_{c_4} = 626$. So the spike train can be divided into six sections where stationarity of the firing rate can be assumed: $\hat{\lambda}_1 = 3.35$, $\hat{\lambda}_2 = 1.18$, $\hat{\lambda}_3 = 3.43$, $\hat{\lambda}_4 = 0.88$, $\hat{\lambda}_5 = 3.65$, $\hat{\lambda}_6 = 2.05$. The fact that the intensity in all sections is comparatively low and the differences between the rates are more likely to be larger (relativ difference is large) indicates that the confidence intervals for the times of the change are tighter i.e. the change points have been accurately pinpointed. In addition, the asymptotic test power is for nearly all window sizes and all $\hat{t}_{c_i}$ bigger than 80%.

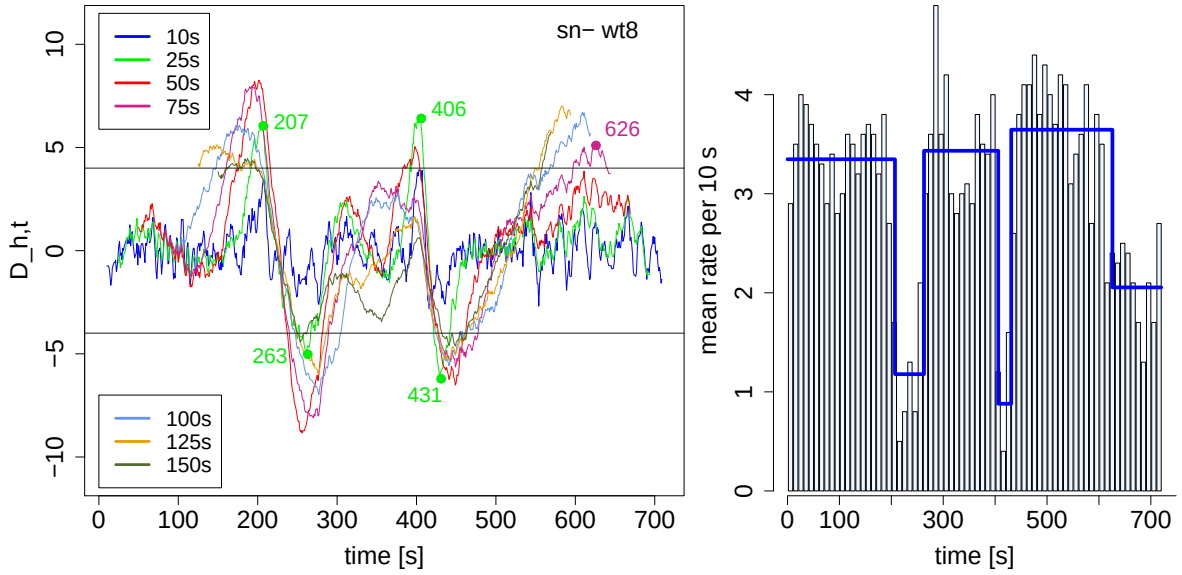

Figure 3.14: Application of the Step-Filter-Test to "sn- wt8". The left picture shows the identified change points. The bar plot on the right presents the average intensity in intervals of length 10s. The blue line marks the estimated step rate function according to the located changes.

3.6 Conclusion of chapter 3

In the present chapter four methods were outlined which share the problem that they provide meaningful illustrations concerning the course of the intensity, but lack the identification of concrete change points and their statistical evaluation.
The method of calculating the empirical variance for different window sizes is not flexible as it is only practicable for some types of spike trains, namely those which include only one rate change or one time scale on which the rate changes several times like every 100 seconds. Otherwise interpretational ambiguity may arise which can lead to a false division of the spike train. As one does not know to which case the spike trains belongs it is impossible to conclude whether the identified h_{max} has to be taken seriously or not. By comparing normed spike counts in overlapping intervals with different lengths, it is possible to draw conclusions about the course of the intensity independent of the type of the rate function. First of all, two graphical methods were developed:

1. Presentation of the normed spike counts in a scatter plot where the abscissa represents the length of the corresponding interval. The colour-code makes it possible to conclude which intensities the first, middle and posterior part contains. But one cannot define exactly the course of the intensity.

2. An improvement was given by connecting those points for which the corresponding intervals have the same centre k. This means that the resulting lines show the

development of the intensity expanding the interval symmetrical around k. So one is able to describe approximately how the intensity changes during the recording. But, it is very complex to define an estimate of the time of the change on the basis of this illustration, as a change in the average intensity of the current interval can be caused from the left and from the right side.

Expanding the interval originating from k only to the right, it is possible to identify the break-points of the corresponding lines which can be taken as candidates for change points in the intensity. For every identified break-point one has to decide whether or not to reject stationarity of the firing rate (null model). This procedure could be constrained to the accumulation points as they are more convincing, but then one has to accept to miss a rate change. The benefit of the method is, that it provides concrete estimates for change points which can be evaluated on the basis of subjective criteria in order to determine which one has to be taken seriously. Problems occur, as not all break-points are unambiguous and in a spike train with stationary firing rate one can also identify break-points which seem to be plausible. Objective criteria are needed to decide if stationarity can be rejected with a high probability. Another problem is that global peaks sometimes cover local peaks so that break-points are not identified and change points missed.

To conclude, all these methods contribute to the detection of rate changes, but it is only possible to evaluate changes in the intensity on the basis of subjective criteria. In comparison to traditional inspections of interspike intervals or average intensities the methods can be rated as more powerful concerning the illustration of changes in the intensity as normed spike counts allow to define characteristic structures like break-points, which make it possible to observe changes in the intensity.

4 Discussion

Spike trains are often considered to arise from stationary point processes whereby the assumption of stationarity is focussed almost exclusively upon the firing rate. As the behaviour of a neuron can change during the course of the observation, most of the models oversimplify the statistics of the investigated spike train. As a consequence, interpretational ambiguity may arise which can lead to biased results in several signal analysis methods. This diploma thesis is concerned with the problem of nonstationarity of the firing rate. The goal was to detect rate changes in spike trains under the assumption that the probability distribution governing the ISIs is exponential and that the spike train can be divided into parts with constant firing intensity.
On the basis of graphical techniques which allow to represent the course of the firing intensity but missed to statistically determine concrete change points, a statistical method is proposed here and developed jointly with a suitable graphical representation of nonstationarity.

4.1 Different approaches for the detection of rate changes

In chapter 3 several techniques for the detection of rate changes were presented. The variance-method is not useful in practice as it only works in special cases like an intensity with one rate change. The other three introduced methods (points, lines, break-points) work with normed spike counts and are built on each other in the way that they represent improvements. They provide impressing illustrations of the intensity and one can learn to interpret the graphics so that the course of the intensity can be reconstructed. However, the determination of the intensity function is partly subjective and time consuming so that in view of the growing amount of spike data the methods are not appropriate.

In chapter 2 a fast and automatic way for the detection of rate changes was established and its performance illustrated. The developed test is based on normed differences

between spike counts in adjacent intervals $[t-h,t]$ and $(t,t+h]$ for different window sizes h and $t \in [h, T-h]$. The test statistic was defined as

$$D_{h,t} = \frac{(N_1 - N_2)}{\sqrt{(N_1 + N_2)}}$$

so that in the case of a stationary Poisson process (null model) the expectation is 0 with variance 1.

The critical value for the decision whether or not to reject the null model was determined in simulations. The criterion was that in 1000 simulated stationary Poisson processes with parameter λ the method observes only in 10 simulations that $D_{h,t}$ crosses the boundary (1%-significant level). The determined critical value was $K = 4$. It has to be taken into account, that the Poisson-assumption is not appropriate for every spike train. In several cases it will be more convincing to approximate the interspike intervals by a gamma distribution with shape parameter κ ($\kappa = 1$ corresponds to the Poisson-model). In comparison to $\kappa = 1$ for $\kappa > 1$ (more regular process) it can be expected that one observes $K < 4$ (1%-significant level) as the occurence of spikes is more regular respectively less variable. As a consequence, $K = 4$ is quite strict when it comes to decide whether or not to reject the null hypothesis so that changes in the intensity are more likely to be missed.

Moreover, the simulated spike trains had all length $T = 700s$, which is approximately the length of the spike trains of the real data, and the window sizes were chosen as $h = 10s, 25s, \ldots, 150s$. This means that the determined boundary is linked to this condition as T and h determine the number of time points t, for which the test statistic can be evaluated e.g. if T is large then there are more time points for which $D_{h,t}$ can be evaluated and this would result in a higher probability of $|D_{h,t}| > K$.

With respect to the application of the method, first of all the size of the windows were defined. The leading point for the choice was the balance between small window sizes (0-100s) to detect short rate sections at all and large window sizes to detect those differences which have otherwise a small probability to be found under the assumption that the rate sections are long enough. In order to have a clear presentation of the results the number of window sizes was restricted.

Finally the choice of the seven window sizes was based on the results of the evaluation of the test power: the chosen window sizes provide an asymptotic test power of 80% for a wide range of rate combinations with $0.8 < \lambda_i < 8$ which are the firing intensities observed in the data. In addition, $h > 150s$ is not absolutely essential because of the strong preconditions: for rate differences which could only be found by $h > 150s$ both rate sections have to be longer than $150s$ as well which does not occur very often as the length of the recording time is $T \approx 720s$.

It has been taken into account, that sometimes a finer adjustment of small window

sizes provides more precise results (see spike train "sn- ko5"). As small window sizes can also detect long rate sections they will always be more important. Large window sizes are only necessary when the rate sections are long and the relative differences between the rates small. A solution would be to separate the illustration of the results and the automatical detection of the rate change like taking several window sizes for a good estimation and afterwords only those curves are illustrated which have detected the change. However, this makes the method more complicated and the illustration contains not the full information any more.
The estimate of the ith change point was defined as $\hat{t}_{c_i}^{h_i^*}$ with h_i^* the smallest window size for which the ith rate change could have been located. Here are other definitions possible like the average over all $\hat{t}_{c_i}^{h_j}$ with $h_1 = 10s, \ldots, h_7 = 150s$ which is too imprecise in several cases as large window sizes are only appropriate for accordingly long rate sections. Another possibility would be to take the estimate of the window size with $\max_h(|D_{h,t}|)$. This might be a problem because not all window sizes are considered so that the optimal window size is not always included in the estimation and therefore it can happen that this definition provides imprecise results.
The quality of the estimate of the change point depends on the hight of rates and the difference between them. The test performs slightly better if the relative difference between the rates is large as the variability of the estimate is small. Note that this has been shown in simulations for a few rate-combinations so that one can only assume a trend.
Having located changes in the intensity, the spike train can be separated into sections where stationarity of the firing rate is justified under the assumption that the intensity is approximately a step rate function. However, for a decreasing (increasing) intensity the estimated step rate function consists of steps with small rate differences ($|\lambda_i - \lambda_{i+1}| < 1$) which are not likely to be pinpointed because of the low test power. Only a rough estimate of the intensity like an approximation by two or three steps might be found (see spike train "sn- wt4"). This depends on the duration of the decrease and on the slope of the rate function. For example, for short sections and slowly decreasing intensities only one rate change might be detected at all.

4.2 Outlook

This diploma thesis provides a first attempt to detect concrete change points in the intensity which enables us to divide the present spike train into parts where stationarity of the firing rate can be assumed. Here, the spike time arrivals were described by a Poisson process which is not always appropriate. The method has to be transferred

to the more general case: the approximation of the interspike intervals by a gamma distribution. Therefore, one has to determine a new boundary K for the decision rule. As it was mentioned before for $\kappa > 1$ one can expect $K < 4$. However, for every shape parameter κ a boundary has to be determined which makes it more complicated as one does not know the true κ and the parameter can change during the course of observation. Further study is necessary in order to investigate if it is possible to expand the method with little effort.

In addition, the problem that a continuous decrease (increase) in the intensity can only poorly be approximated by a step rate function has to be tackled. Maybe the comparison of two adjacent intervals has to be extended, so that the difference during the decrease gets more conspicuous.

In summary, the Step-Filter-Test is an easily applicable method to statistically determine concrete change points in the firing intensity jointly with a suitable graphical presentation. It could be used as preprocessing method, in order to handle the problem of nonstationarity of the firing rate when analysing spike trains.

Bibliography

Baker, S. (2000). An accurate measure of the instantaneous discharge probability, with application to unitary joint-event analysis. *Neural Computation*, 12:647–669.

Brody, C. (1999). Correlations without synchrony. *Neural Computation*, 11:1537–1551.

Gourevitch, B. and Eggermont, J. (2007). A simple indicator of nonstationarity of firing rate in spike trains. *Journal of Neuroscience Methods*, 163:181–187.

Gutkin, B. and Ermentrout, G. (2006). Spikes too kinky in the cortex? *Nature*, 440:999–1000.

Haken, H. (2008). *Brain dynamics*. Berlin, Heidelberg: Springer.

Hanslmayr, S., Aslan, A., Staudigl, T., Klimesch, W., Herrmann, C., and Bäuml, K. (2007). Prestimulus oscillations predict visual perception performance between and within subjects. *Neuroimage*, 37:1465–1473.

Nawrot, M., Boucsein, C., Molina, V., Riehle, A., Aertsen, A., and Rotter, S. (2008). Measurement of variability dynamics in cortical spike trains. *Journal of Neuroscience Methods*, 169:374–390.

Perkel, D., Gerstein, G., and Moore, G. (1967). Neuronal spike trains and stochastic point processes. the single spike train. *Biophysical Journal*, 7:391–417.

Ringach, D. (2009). Spontaneous and driven cortical activity: implications for computation. *Current Opinion in Neurobiology*, 19:439–444.

Shimokawa, T., Koyama, S., and Shinomoto, S. (2009). A characterization of the time-rescaled gamma process as a model for spike trains. *Journal of Computational Neuroscience*.